Inorganic Chemistry
Article
Cite This: Inorg. Chem. XXXX, XXX, XXX−XXX
pubs.acs.org/IC

Near-IR/Visible-Emitting Thiophenyl-Based Ru(II) Complexes: Efficient Photodynamic Therapy, Cellular Uptake, and DNA Binding

Si-Qi Zhang,[†] Ting-Ting Meng,[†,∥] Jia Li,[§] Fan Hong,[§] Jin Liu,[§] Youjun Wang,[§] Li-Hua Gao,[‡] Hua Zhao,[‡] and Ke-Zhi Wang*[,†]

[†]Key Laboratory of Radiopharmaceuticals, Ministry of Education, College of Chemistry, Beijing Normal University, Beijing 100875, People's Republic of China

[‡]School of Science, Beijing Technology and Business University, Beijing 100048, People's Republic of China

[§]Beijing Key Laboratory of Gene Resource and Molecular Development, Beijing Normal University, Beijing 100875, People's Republic of China

[∥]College of Science, Liaoning Technical University, Fuxin 123000, People's Republic of China

Supporting Information

ABSTRACT: Near-IR-emitting and/or efficiently photodynamic water-soluble Ru(II) complexes that hold great application potentials as photodynamic therapy and/or photodetection agents for cancers have been poorly explored. In this paper, the solvatochromism, calf thymus DNA binding, and singlet oxygen generation properties of a known ruthenium(II) complex of visible-emitting $[Ru(bpy)_2(dtdpq)](ClO_4)_2$ (**Ru1**) and a new homoleptic complex of near-IR-emitting $[Ru(dtdpq)_3](ClO_4)_2$ (**Ru2**) (bpy = 2,2′-bipyridine, dtdpq = 2,3-bis(thiophen-2-yl)pyrazino[2,3-*f*][1,10]phenanothroline) in water are reported. Moreover, DNA photocleavage, singlet oxygen generation in HeLa cells, cellular uptake/localization, and in vitro photodynamic therapy for cancer cells of water-soluble **Ru1** are described in detail. The results show that **Ru1** acted as potent photodynamic cancer therapy and mitochondrial imaging agents. **Ru2** exhibited very strong solvatochromism from a visible emission maximum at 588 nm in CH_2Cl_2 to the near-IR region at 700 nm in water and singlet oxygen generation yield in water (23%) and DNA binding properties (intercalative DNA binding constant on the order of 10^6 M^{-1}) comparable to those of **Ru1**, which should make **Ru2** attractive for the aforementioned applications of **Ru1** if the water solubility of **Ru2** can be improved enough for the studies above.

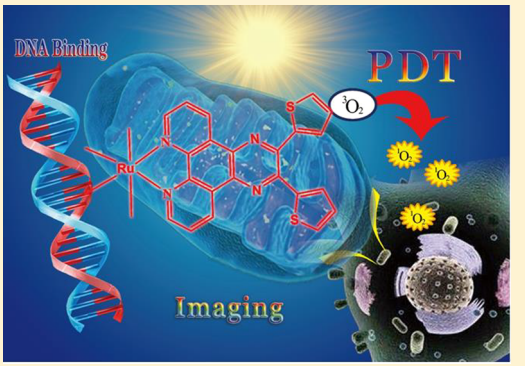

INTRODUCTION

Cancer has become the second leading cause of death, followed by ischemic heart disease, and it is predicted that new cancer cases will increase to more than 27 million by 2030.[1,2] Photodynamic therapy (PDT), as an emerging medical technique, has evolved into a successful alternative or complementary treatment to some traditional therapeutic methods (e.g. radiotherapy, chemotherapy, and tumor surgical resection) to fight against cancer, because of the superior noninvasive character of PDT agents which are able to provide spatial and temporal control over cancer cell killing.[3−5] An ideal PDT agent requires[6−8] (1) high solubility and photostability in aqueous media, (2) strong absorption in phototherapy windows, (3) long excited state lifetime, (4) ability to rapidly enter cells, (5) inactivity in the dark, and (6) high singlet oxygen ($^1O_2$) quantum yields on exposure to light. Upon irradiation, the nontoxic (or low-toxicity) photosensitizer (PS) is excited from its ground state S_0 to the first excited state S_1 and subsequently to the triplet state T_1 via nonradiative intersystem crossing (ISC) and then transfer electrons and/or energy to ground-state molecular oxygen ($^3O_2$) to generate cytotoxic reactive oxygen species (hydroxyl radical, superoxygen anion radical) (type I) and/or $^1O_2$ (type II), which ultimately induce cancer cell damage.[8−11] Photofrin, a complex mixture of monomeric and oligomeric porphyrins, is the first generation PS that was approved by the U.S. Food and Drug Administration for clinical application in the treatment of variety of cancers such as neck, head, and esophageal.[12] However, the lack of chemical homogeneity and stability, low cell uptake and retention, and skin phototoxicity make the treatment painful for patients.[13] In the search for metal-based PSs against cancer, Ru(II) polypyridyl complexes play an important role because of their advantages such as high chemical and photochemical stabilities, excitation and emission in the visible/near-IR window and extended π systems that facilitate $^1O_2$ generation in high yield.[5,8,14] **TLD-1433** ($[Ru(dmb)_2(ttip)]Cl_2$; dmb = 4,4′-dimethyl-2,2′-bipyridine; ttip = 2(2-(2′,2″:5″,2‴-terthiophene)imidazo[4,5-*f*][1,10]-phenanthroline) is the first Ru(II)-based photosensitizer

Received: August 12, 2019

DOI: 10.1021/acs.inorgchem.9b02420
Inorg. Chem. XXXX, XXX, XXX−XXX

Scheme 1. Chemical Structures of Complexes Ru1 and Ru2

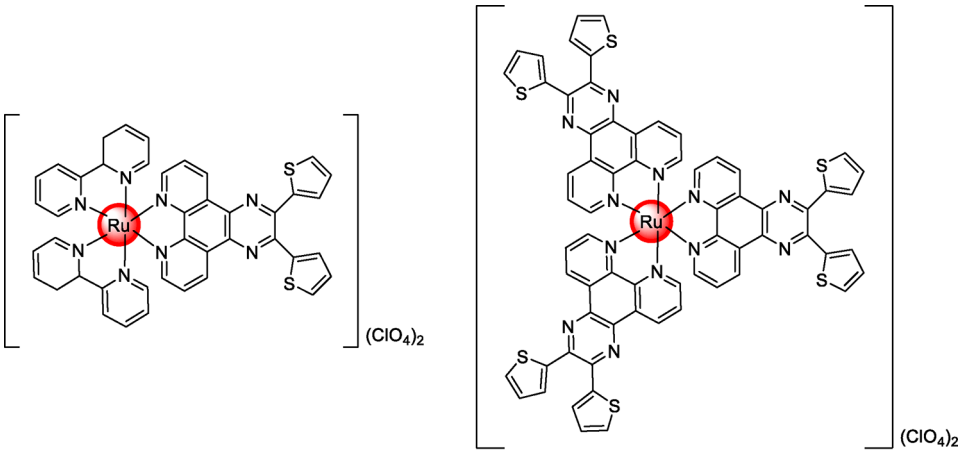

$[Ru(bpy)_2dtdpq](ClO_4)_2$ **Ru1**

$[Ru(dtdpq)_3](ClO_4)_2$ **Ru2**

applied to PDT and has advanced to Phase Ib clinical trials against invasive bladder cancer.[15,16] Thiophene-containing polypyridyl Ru(II) complexes represent one class of PSs with extremely high $^1O_2$ quantum yields and have the potential to be used as a new generation of PDT drugs.[17,18] Alberto et al.[19] reported a careful DFT and TDDFT investigation of the influence of thiophene units on the $^1O_2$ generation of polypyridyl Ru(II) complexes containing polythiophene chains of different lengths, and the results suggested that the increasing number of thiophene units (n = 3, 4) afforded a very low lying state which could be populated by an ISC mechanism and promoted $^1O_2$ generation to exert their PDT effect. These Ru(II) complexes are superior to Photofrin and are undergoing the human Phase I studies with the photodynamic index increasing with increasing thiophenyl group number n, 0 (ϕ = 0.5, n = 1), > 1.8 (ϕ = 0.75, n = 2), 10 (ϕ = 1, n = 3), to >200 (ϕ = 1, n = 4), against HL-60 cells upon irradiation with 7 J cm^{-2} of visible light.[20] We have reported a series of thiophenyl-containing Ru(II) complexes and found that the introduction of the thiophenyl group significantly enhanced DNA binding and photocleavage properties as well as the acidity of Ru(II) complex.[21−24]

DNA is an important genetic material and is considered to be the primary target for many metal-based anticancer drugs. A small conformational change of its double helix could perturb the orderly progress of DNA replication, transcription, and repair.[25−27] Therefore, it is undoubtedly important to discover novel DNA binders as nucleic acid probes for life process exploration, disease diagnosis, and therapy. Some Ru(II) complexes have been discovered to serve as DNA photocleavage reagents, nucleic acid sequence-specific and mismatch luminescent probes, and antitumor agents.[28−31] Among these Ru(II) complexes, DNA intercalative $[Ru(bpy)_2(dppz)]^{2+}$ (dppz = dipyrido[3,2-*a*:2′3′-c]phenazine) is one of the most well-known molecular "light switches" for DNA because of its evident photophysical changes that display no photoluminescence in aqueous solution but dramatic emission enhancement in the presence of DNA.[32] Since the discovery of $[Ru(bpy)_2(dppz)]^{2+}$, tremendous attention has paid to dppz derivative based Ru(II) complexes. Evidence shows that electron effects, planarity, and hydrophobicity of substituent groups on dppz units play important roles in the DNA binding properties, including DNA binding affinities, thermal stabilization effects, DNA photocleavage, binding selectivity and kinetics, cellular uptake/localization, dark cytotoxicities, and PDT effects.[6,33−36] However, Ru(II) complexes with an organic ligand analogous to dppz, dipyrido[6,7-d:2′3′-*f*]-quinoxaline (dpq), have received much less attention. Delaney and Aldrich-Wright first reported the synthesis and DNA affinity of $[Ru(bpy)_2dqp]^{2+}$ [37] and $[Ru(dpq)_3]^{2+}$ [38] in 2002 and 1995, respectively. It was reported that $[Ru(phen)_2(dpq)]^{2+}$ and $[Ru(phen)_2(Me_ndpq)]^{2+}$ (n = 1, 2; Medpq = 2-methyldipyrido[3,2-*f*:2′,3′-*h*]quinoxaline; Me_2dpq = 2,3-methyldipyrido[3,2-*f*:2′,3′-*h*]quinoxaline) exhibit no DNA light-switch behavior, since strong luminescence of these complexes in both the absence and the presence of DNA were observed.[39−41] In contrast, $[Ru(phen)_2(dicnq)]^{2+}$ and $[Ru(phen)(dicnq)_2]^{2+}$ (dicnq = 6,7-dicyanodipyrido[2,2-*d*:2′,3′-*f*]quinoxaline) were reported to act as DNA molecular light switches with 16- and 8-fold luminescence enhancement, respectively.[42] More interestingly, the grafting of an amide group to dpq caused a significant effect on the excited-state properties of the Ru(II) complex $[Ru(phen)_2dpqa]^{2+}$ (dpqa = 2-pentylamidodipyrido[3,2-*f*:2′,3′-*h*]quinoxaline), which showed impressive DNA molecular light-switching properties.[39] We have also reported the four DNA molecular light-switch complexes $[Ru(phen)_2(Hcdpq)](ClO_4)_2$ (phen = 1,10-phenanthroline, Hcdpq = 2-carboxyldipyrido[3,2-*f*:2′,3′-*h*]-quinoxaline), $[Ru(bpy)_2(bipp)]^{2+}$ (bipp = 2-benzimidazoylpyrazino[2,3-*f*][1,10]phenanthroline), $[Ru(bpy)_2(bopp)]^{2+}$ (bopp = 2-benzoxazolylpyrazino[2,3-*f*]-[1,10]phenanthroline), and $[Ru(bpy)_2(btpp)]^{2+}$ (btpp = 2-benzthiazolylpyrazino[2,3-*f*][1,10]phenanthroline), which were synthesized by grafting of carboxyl group, benzimidazoyl, benzoxazolyl, and benzthiazolyl moieties to $[Ru(bpy)_2(dpq)]^{2+}$ with ct-DNA-induced emission enhancement factors of 26-, 49-, 89-, and 179-fold, respectively.[43,44] It should be pointed out that most early studies on Ru(II) complexes have focused on their electrochemical properties, potencies as traditional cytotoxic agents, and in vitro interactions with DNA and have made remarkable achievements.[45−47] In recent years, attention has shifted to cellular uptake, subcellular localization, and photocytotoxicity properties of Ru(II) complexes, along with the mechanisms of their various biological behaviors, providing a deeper understanding of the action mechanisms of

DOI: 10.1021/acs.inorgchem.9b02420
Inorg. Chem. XXXX, XXX, XXX−XXX

these complexes and promoting their clinical transformation.[7,48,49]

During our exploration of the influences of thiophenyl substitution on dpq-based Ru(II) complexes on their DNA binding and photocleavage properties as well as their PDT effects of Ru(II) complexes, we have found some encouraging results on $[Ru(bpy)_2(dtdpq)](ClO_4)_2$ (**Ru1**) and $[Ru(dtdpq)_3](ClO_4)_2$ (**Ru2**) (bpy = 2,2′-bipyridine, dtdpq = 2,3-bis(thiophen-2-yl)pyrazino[2,3-*f*][1,10]phenanothroline) (see Scheme 1): (1) the introduction of dithiophenyl groups evidently enhances DNA binding, DNA photocleavage, and singlet oxygen generation ability, (2) **Ru2** in water is strongly emissive in the near-IR region with sensitive solvatochromism, and (3) **Ru1** is a promising mitochondrial imaging and PDT cancer therapy difunctional agent. Herein we demonstrate these interesting findings.

EXPERIMENTAL SECTION

Materials and Characterization. **Ru1** was synthesized according to a modified literature method,[3] while **Ru2** is a new compound; their synthetic details and characterization data are shown in the Supporting Information.

DNA Photocleavage Experiments. The photoinduced DNA cleavage by Ru(II) complexes was carried out by agarose gel electrophoresis. Supercoiled pUC18 DNA (0.2 μg) was treated with different concentrations of Ru(II) complexes in buffer A (5 mM Tris-HCl, 50 mM NaCl, pH 7.1 ± 0.02), and then the mixture was irradiated with UV light (360 nm) for 1 h at room temperature. The samples were subjected to electrophoresis on a 1.0% agarose gel in TAE buffer (40 mM Tris, 20 mM acetic acid, 1 mM EDTA, pH 8.0) at 120 V and 80 mA for 50 min. The gel was stained with 1 μg/mL of EB solution and photographed for analysis with a gel imager. The percentage of cleavage (C) was calculated according to eq 1[23,24]

$$C\ (\%) = \frac{D_{II} + 2D_{III}}{D_I + D_{II} + 2D_{III}} \times 100\% \quad (1)$$

where D_I, D_{II}, and D_{III} represent the integrated density values of form I (supercoil), form II (nicking form), and form III (linear form), respectively.

Quantum Yields for Singlet Oxygen Generation. The fluorescence quantum yields for $^1O_2$ production of **Ru1** and **Ru2** under irradiation were measured by using anthracene-9,10-dipropionic acid disodium salt (ADPA) as the $^1O_2$ indicator and rose bengal in PBS as the standard photosensitizer.[34] ADPA reacts irreversibly with $^1O_2$, leading to a decrease in its absorbance at 378 nm; therefore, $^1O_2$ can be detected quantitatively by monitoring the decrease in the absorbance of ADPA. Briefly, ADPA (9 μM) was mixed with Ru(II) complexes or RB in PBS and irradiated with 66 mW/cm^2 white light for 10 min. The absorbances of ADPA at 378 nm were recorded after sufficient mixing at a specific time interval of 1 min. The quantum yields for $^1O_2$ generation of **Ru1** and **Ru2**, Φ_{Ru}, were calculated according to eq 2 using RB as a standard (Φ_{RB} = 0.75)[50]

$$\Phi_{Ru} = \frac{\Phi_{RB} K_{Ru} A_{RB}}{K_{RB} A_{Ru}} \quad (2)$$

where K_{Ru} and K_{RB} are the photodegradation rate constants of ADPA at 378 nm by light irradiation in the presence of the Ru(II) complex and RB, respectively, and A_{Ru} and A_{RB} stand for integral areas of absorption peaks in the range of 400−700 nm for the Ru complex and RB, respectively.

In Vitro Dark Cytotoxicity and PDT Therapy. The dark cytotoxicity and phototoxicity of **Ru1** and **Ru2** were evaluated by an MTT assay against human cervical cancer (HeLa), lung cancer (A549), and breast cancer (MCF-7) cell lines. Cells were seeded in 96-well plates at a density of 4 × 10^3 cells/well and incubated overnight. Stock solutions of **Ru1** and **Ru2** were freshly prepared in dimethyl sulfoxide (DMSO) and diluted with DMEM culture media to the desired concentrations. After that, cells were incubated with 100 μL of culture media containing serial concentrations of **Ru1** and **Ru2**. The dark cytotoxicity was assessed after incubation without any irradiation for 48 h. For the photocytotoxicity study, on incubation for 12 h, the cells were irradiated using visible light (400−700 nm) at a power of 25.4 mW/cm^2 for 13, 20, and 30 min, respectively. After the cells were grown for another 36 h, 10 μL of MTT solution (50 μg/mL) was added to each well for 4 h. Then the medium containing unreacted MTT was removed carefully, followed by addition of 200 μL of DMSO to dissolve the blue formazan. The optical density (OD) at 570 nm was measured with a microplate reader. The percentage of cell viability was calculated with eq 3:

$$\text{cell viability}\ (\%) = \frac{\text{OD value of test}}{\text{OD value of control}} \times 100 \quad (3)$$

Cellular Uptake. HeLa cells were plated on six-well plates and maintained at 37 °C under a 5% CO_2 atmosphere overnight. To evaluate concentration-dependent intracellular incorporation, different concentrations (5, 10, 20, 40, 80 μM) of **Ru1** were added and incubated for 6 h. To assess the dependence of incubation time, 20 μM of **Ru1** was added in culture medium for 0.25, 0.5, 1, 2, 4, and 6 h. After the incubation time, cells were harvested and washed three times with PBS. Finally, the fluorescence intensity of cells containing **Ru1** was measured using a flow cytometer (NovoCyte). The fluorescence emission channel setting was 615 ± 10 nm.

Confocal Laser Scanning Microscopy (CLSM). HeLa cells (1 × 10^4 cells/mL) were seeded in 35 mm glass-bottom culture dishes and treated with 20 μM **Ru1** for 2 h. Before imaging, the cells were further incubated with LysoTracker Green (200 nM) and MitoTracker Green (200 nM) for 0.5 h, followed by washing three times with phosphate buffer solution (PBS) (pH 7.4). Confocal images were obtained by a Nikon A1MP confocal microscope using a 60× oil objective at an excitation of λ_{ex} = 488 nm. The emissions were collected at 640−720 nm for ruthenium(II) complexes and 505−530 nm for Tracker Green.

Apoptosis Detection. Apoptosis was detected by mean of FITC staining. HeLa cells were seeded in 35 mm culture dishes at a density of 5 × 10^4 cells for 24 h before treatment. The medium was replaced with **Ru1** of different concentrations in DMEM for 12 h and then irradiated with viable light (25.4 mW/cm^2). The cells were stained with Annexin V-FITC according to the manufacturer's instructions.

Cellular Signal Oxygen Detection. HeLa cells were seeded in six-well plates at a density of 5 × 10^4 cells per well. After treatment with **Ru1** at the indicated concentrations for 12 h, the cells were incubated with 10 μM of 2′,7′-dichlorodihydrofluorescein diacetate (DCFH-DA) dye for 20 min in the dark and then irradiated with 25.4 mW/cm^2 visible light for 13 min and rinsed three times with serum-free DMEM. NaN_3 (10 mM), used as an inhibitor of ROS, was added to certain wells 1 h before irradiation. Fluorescence images of samples were captured by inverted fluorescence microscopy. The fluorescence intensity of DCF in HeLa cells was detected using flow cytometry (NovoCyte).

RESULTS AND DISCUSSION

Synthesis and Characterization. The thiophenyl-containing ligand dtdpq and its two Ru(II) complexes **Ru1** and **Ru2** were synthesized according to the routes shown in Schemes S1−S3 (Supporting Information), and the synthetic details are provided in Supporting Information. dtdpq was synthesized by condensation of 1,10-phenanthroline-5,6-diamine with 2-bis(thiophen-2-yl)ethane-1,2-dione in the presence of acetic acid as the solvent and was authenticated by ^{1}H NMR spectroscopy (see Figure S1a in the Supporting Information). During the time we carried out this study, the synthesis and study on the azo dye decomposition of **Ru1** were reported.[3] Here **Ru1** was synthesized in a moderate yield of 55% by reacting equimolar dtdpq and $Ru(bpy)_2Cl_2·2H_2O$ in refluxing *N*,*N*-dimethylformamide for 8 h; the crude product

DOI: 10.1021/acs.inorgchem.9b02420
Inorg. Chem. XXXX, XXX, XXX−XXX

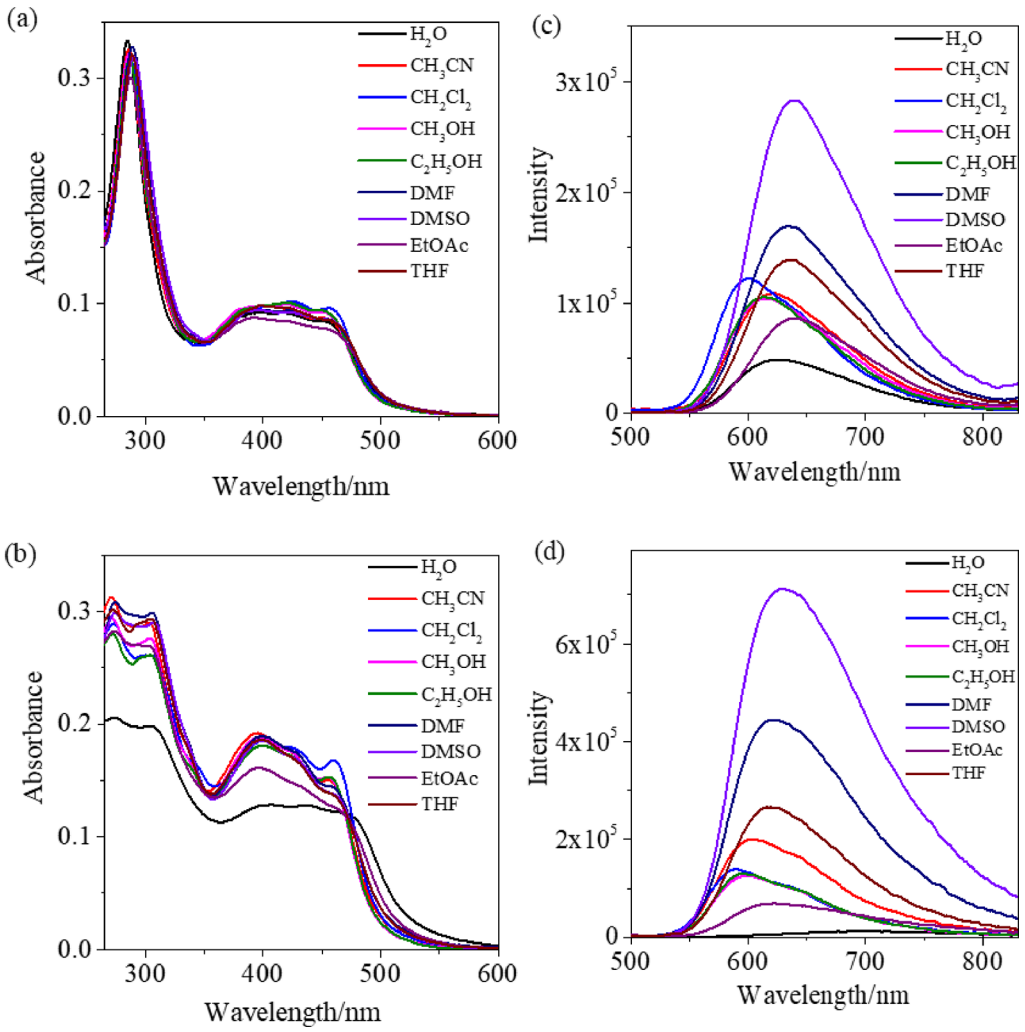

Figure 1. Absorption spectra of **Ru1** (a) and **Ru2** (b) and emission spectra of **Ru1** (c) and **Ru2** (d) in different solvents at 298 K.

was purified by chromatography over silica gel using CH_3CN/H_2O/saturated potassium nitrate aqueous solution (v/v/v, 50/5/1) as the eluent and recrystallized by diffusion of diethyl ether into an acetonitrile solution of **Ru1**. In addition to the data of satisfactory CHN elemental analyses, consistent proton intergral areas corresponding to the presence of 28 protons (see Figure S1b in the Supporting Information) and a positive ion electrospray ionization (ESI) mass spectrum (see Figure S1c, Supporting Information) showed peaks at m/z 405.08 and 909.14 which were assigned to $[M - 2ClO_4^-]^{2+}$ and $[M - ClO_4^-]^+$, respectively. **Ru2** was synthesized in a moderate yield of 63% by reacting dtdpq and $RuCl_3 \cdot H_2O$ in a 3:1 molar ratio in refluxing ethylene glycol for 10 h; the crude product was chromatographed over silica gel using CH_2Cl_2/CH_3OH/DMF (v/v/v, 5/1/0.5) as the eluent and recrystallized by diffusion of diethyl ether into an acetonitrile solution of **Ru2**. The formation of homoleptic **Ru2** was authenticated by elemental analyses, ^1H NMR (see Figure S2a in the Supporting Information), and mass spectrometry (see Figure S2b in the Supporting Information) as well. As anticipated, **Ru2** showed much simplified ^1H resonance peaks that are similar to those of free dtdpq (see Figure S1a in the Supporting Information) due to the equal distribution of three dtdpq groups around the Ru center, in comparison to **Ru1**. The molecular ion peak centered at m/z 645.9 (calculated value m/z 645.2) in its positive ion ESI mass spectrum is ascribed to $[M - 2ClO_4^-]^{2+}$.

Solvatochromism. The absorption and emission spectra for **Ru1** and **Ru2** measured in various polar and nonpolar solvents at room temperature are shown in Figure 1, and the corresponding photophysical data are given in Table S1 (Supporting Information). Both complexes display high molar extinction coefficients. **Ru1** exhibits a small shift in absorption maxima in all the solvents used, which indicates a weak interaction between **Ru1** and the investigated solvents at the ground state. The absorption spectrum of **Ru2** in aqueous solution is significantly different from those in other solvents. The high-intensity absorption bands in the UV region (200–350 nm) are assigned to ligand to ligand charge transfer (LLCT; $\pi-\pi^*$) transitions, and the moderately strong absorption bands and shoulders in the visible region (350–500 nm) originate from singlet metal to ligand charge transfer (^{1}MLCT) transitions. Upon excitation at the ^{1}MLCT absorption wavelength, a strong solvatochromism was observed for **Ru2** from CH_2Cl_2 (588 nm) to H_2O (700 nm), suggesting a significantly strong solvent–complex interaction at the excited state. Such a large red shift has rarely been reported in Ru(II) complexes[51−54] and is much more evident than a red shift of only about 25 nm observed for the emission of **Ru1** from CH_2Cl_2 (600 nm) to H_2O (625 nm)

DOI: 10.1021/acs.inorgchem.9b02420
Inorg. Chem. XXXX, XXX, XXX−XXX

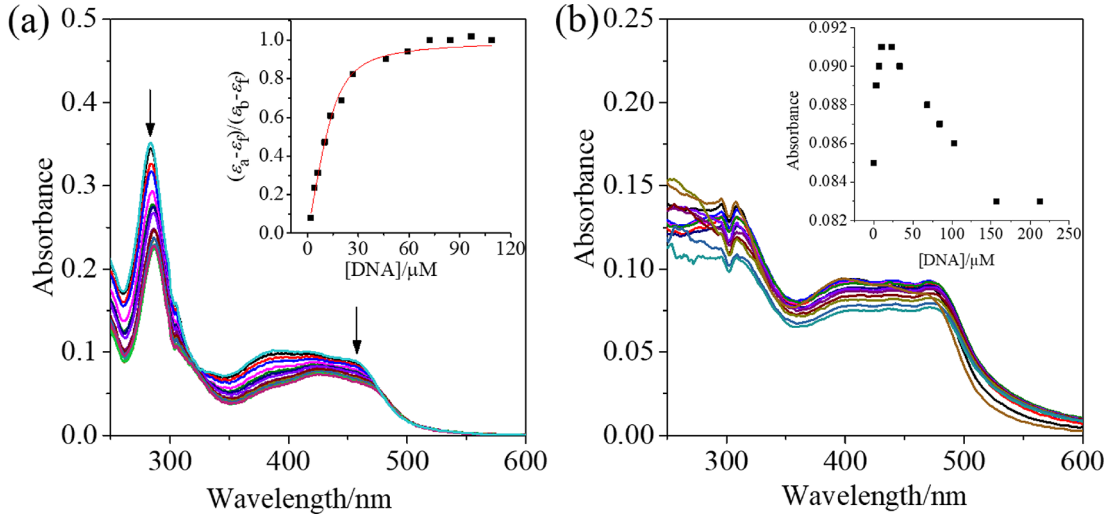

Figure 2. Absorption spectra of Ru(II) complexes in the presence of various amounts of CT-DNA: (a) **Ru1** (3.98 μM), [DNA]/[Ru] = 0.00–27.38; (b) **Ru2** (2.33 μM), [DNA]/[Ru] = 0.00–90.99.

and even a maximum red shift of 40 nm from CH_2Cl_2 (600 nm) to EtOAc (640 nm). The luminescence quantum yields of **Ru1** and **Ru2** were measured using $[Ru(bpy)_3]^{2+}$ in water as a standard. **Ru1** and **Ru2** in DMSO displayed the lowest-energy emission maxima at 639 and 629 nm and maximum emission quantum yields of 0.052 and 0.087, respectively. It is noteworthy that the NIR emission of **Ru2** in water with a medium quantum yield of 0.134% is interesting and encouraging, since NIR emission (700–2500 nm) has become a challenging research field with widespread potential applications in optical sensing, bioimaging, NIR light-emitting diodes, telecommunications, and night-vision-readable displays.[55,56] To date, NIR-emitting mononuclear tris(bidentate NN ligand)-based Ru(II) complexes are rather lacking.[31,57–59] In order to verify whether or not the severe aggregation due to the poor water solubility of **Ru2** was the origin of its NIR emission in water, we have checked the effects of volume percentage of CH_3CN in CH_3CN/H_2O mixed solvents on the emission spectra of **Ru2**. We found that the emission intensities at 700 nm slightly increased upon increasing CH_3CN from 0% up to 14%, while intensities of a new emission peak at ~604 nm were evidently enhanced by ~10-fold upon further gradual increases in the CH_3CN contents to 25% (figure not shown). The aforementioned observations indicated that the aggregation would not make a dominant contribution to the NIR emission of **Ru2**, and the real origin needs further studies.

Calf Thymus DNA Binding Effects on UV–Visible and Emission Spectra. The DNA binding of complexes through intercalation usually leads to hypochromism H% (H% = $(A_{free} - A_{bound})/A_{free} \times 100\%$) and bathochromism ($\Delta\lambda$), because the intercalative mode involves a strong $\pi-\pi$ stacking interaction between the aromatic chromophore of the complexes and the base pairs of DNA.[60] In this study, we added increasing amounts of CT-DNA to buffer A containing **Ru1** (3.98 μM) or **Ru2** (2.33 μM), and subsequently their absorption spectra were measured after sufficient mixing for 5 min (Figure 2). For **Ru1**, in the presence of successive increases of the DNA (from 0.00 to 109 μM), the bands at both 284 and 455 nm showed apparent decays with hypochromisms H% of about 36% and 26% and red shifts of 3 and 5 nm, respectively. In contrast, DNA binding to **Ru2** induced nonmonotonic spectral changes: decreases and increases in the absorption intensities over the low and high DNA concentrations. This DNA binding induced two-stage UV–vis spectral change is similar to those we previously observed for the binding of $[Ru(bpy)_2(btppz)]^{2+}$ (btppz = benzo[h]tripyrido[3,2-a:2′,3′-c:2″,3″-j]phenazine) to DNA[61] and may be due to the two different DNA binding conformations. This complex spectral behavior prevents us from deriving the DNA binding constant of **Ru2**. The intrinsic DNA binding constant K_b and binding site size s of **Ru1** were calculated to be $(1.51 \pm 0.51) \times 10^6$ M^{-1} and 2.05 ± 0.23, respectively, by monitoring the intensity change at 455 nm, according to eqs 4 and 5

$$(\varepsilon_a - \varepsilon_f)/(\varepsilon_b - \varepsilon_f) = [b - (b^2 - 2K_b{}^2C_t[\mathrm{DNA}]/s)^{1/2}]/(2K_bC_t) \quad (4)$$

$$b = 1 + K_bC_t + K_b[\mathrm{DNA}]/2s \quad (5)$$

where [DNA] is the concentration of DNA in base pairs, C_t is the total Ru(II) complex concentration, ε_a corresponds to apparent extinction coefficients of the Ru(II) complex and ε_b and ε_f are the extinction coefficients for the ruthenium complex in the fully bound form and the free form, respectively. The DNA binding strength of **Ru1** is comparable to those of the typical DNA intercalators $[Ru(bpy)_2(dppz)]^{2+}$ (1.2×10^6 M^{-1}) and ethidium bromide (1.25×10^6 M^{-1}),[51] indicating that **Ru1** might be a strong DNA intercalator. In order to compare quantitatively the DNA-binding properties with analogous complexes, their DNA binding parameters are given in Table 1. It is noteworthy that the DNA-binding affinity of **Ru1** is 5-fold as greater than the K_b value of 3.2×10^5 M^{-1} for the parent complex $[Ru(bpy)_2dpq]^{2+}$,[62] which is beyond our anticipation since the thiophene units are twisted significantly from the parent dpq plane, as revealed by the reported structural parameters.[3,63] Thus, it is anticipated that the structure of **Ru1** in the crystalline form would be different from that in the DNA-bound form, in which the thiophene units are coplanar with the parent dpq, so that the more extended conjugation plane of dtdpq in comparison to dpq conforms to the general trend that Ru(II) complexes with a more extended aromatic plane would bind to the DNA more

DOI: 10.1021/acs.inorgchem.9b02420
Inorg. Chem. XXXX, XXX, XXX–XXX

Table 1. Comparison of DNA-Binding Data for Ru1 and Ru2 with Those for Analogous Ru(II) Complexes[a]

complex	K_b (10^5 M^{-1})	$\Delta\lambda$/nm	hypochromism H% (λ/nm)	ref
$[Ru(bpy)_2(dppz)]^{2+}$	12	0	18 (445)	64
$[Ru(bpy)_2(dpq)]^{2+}$	3.2	0	21(442)	62
$[Ru(bpy)_2(dicnq)]^{2+}$	3.7	0	12 (449)	62
$[Ru(bpy)_2(dppp2)]^{2+}$	5.2	2	11(440)	62
$[Ru(bpy)_2(dppp3)]^{2+}$	4.8	1	14(442)	62
$[Ru(bpy)_2(dmdpq)]^{2+}$	0.23	0	11(453)	60
$[Ru(bpy)_2dtdpq]^{2+}$	15.1	5	26(455)	this work
$[Ru(dtdpq)_3]^{2+}$	1.24			this work

[a]The structures are as follows:

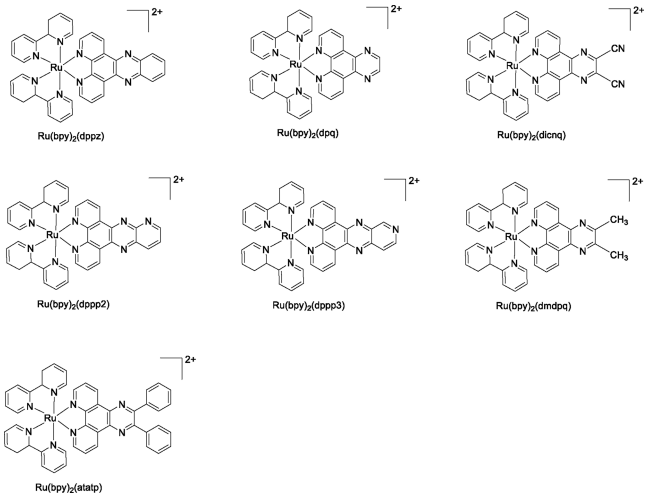

deeply and tightly.[64,65] The absorption intensification at the lower DNA concentrations in the DNA-induced nonmonotonic spectral changes, shown in the inset to Figure 2b, may correspond to such a conformation change from a nonplanar state of thiophene groups and dpq to a coplanar state of these two moieties, resulting in enhanced conjugation and accordingly the enhanced absorption intensities. The possibility that H bonds formed between H atoms of DNA base pairs and the pyridine N atoms of $[Ru(bpy)_2(dppp2)]^{2+}$ (dppp2 = pyrido[2′,3′:5,6]pyrazino[2,3-*f*][1,10]-phenanthroline) and [Ru(bpy)$_2$(dppp3)]2+ (dppp3 = pyrido-[3′,4′:5,6]pyrazino[2,3-*f*][1,10]phenanthroline) hinder dppp2 and dppp3 from inserting into the DNA[62] could be ruled out in **Ru2**.

Luminescence spectroscopy was also used to characterize the DNA-binding properties of **Ru1** and **Ru2**. As shown in Figure 3a, in the absence of DNA, **Ru1** emitted weak luminescence (quantum yield ϕ = 0.789% at λ_{max} = 625 nm) in aqueous buffer but increased sharply upon addition of CT-DNA with a maximum intensity enhancement factor (I/I_0) of 10.5, implying that **Ru1** acted as a good DNA molecular light switch. This factor is only modest in comparison to the factors of 8, 16, >50, 6, 50, 90, and 180 previously reported for $[Ru(phen)(dicnq)_2]^{2+}$, $[Ru(phen)_2(dicnq)]^{2+}$,[42] $[Ru(phen)_2dpqa]^{2+}$ (dpqa = 2-pentylamidodipyrido[3,2-*f*:2′,3′-*h*]-quinoxaline),[66] $[Ru(phen)_2(dpq)]^{2+}$,[41] $[Ru(bpy)_2(bipp)](ClO_4)_2$, $[Ru(bpy)_2(bopp)](ClO_4)_2$, and $[Ru(bpy)_2(btpp)](ClO_4)_2$,[67] respectively. The following possible causes were reported for the DNA light switching effects observed:[32,68−71] (1) the intercalative group was protected from forming intermolecular hydrogen bonds of the N moieties with water or excited-state proton transfer from the solvent water to the N moieties, (2) a hydrophobic environment provided by the DNA decreases radiative vibrational relaxation, and (3) the presence of a bright ^{3}MLCT state and a dark ^{3}MLCT state and DNA binding results in a more populated bright ^{3}MLCT state, which enhances the luminescence of the Ru(II) complexes. However, successive additions of DNA (0.00−90 μM) into **Ru2** (2.33 μM) elicited slight emission enhancement by a factor of 1.32 along with a blue shift by 30 nm from 700 to 670 nm (see Figure 3b). This large DNA binding induced blue shift is not common in comparison to previously reported near-IR-[72−74] and visible-light-emitting Ru complex based DNA intercalators and groove binders[75] and has not been observed for any DNA electrostatic binders.[76,77] This DNA binding

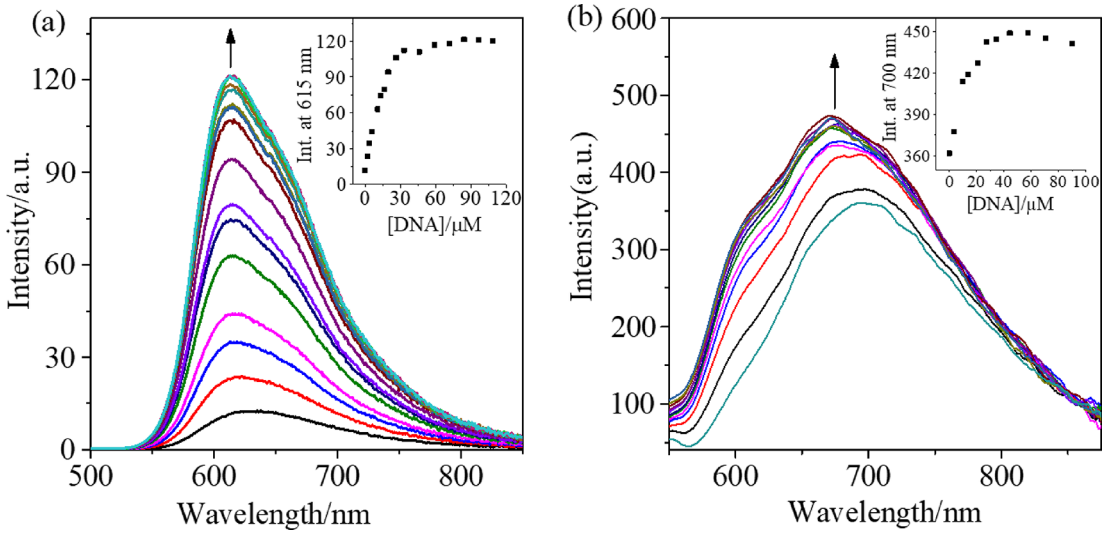

Figure 3. Changes in the luminescence spectra of Ru(II) complexes in 5 mM Tris-HCl and 50 mM NaCl buffer (pH 7.2) in the presence of increasing concentrations of ct-DNA: (a) **Ru1** (3.98 μM), ct-DNA (0.00−109 μM); (b) **Ru2** (2.33 μM), ct-DNA (0.00−90 μM). Arrows show the intensity changes upon increasing DNA concentration.

DOI: 10.1021/acs.inorgchem.9b02420
Inorg. Chem. XXXX, XXX, XXX−XXX

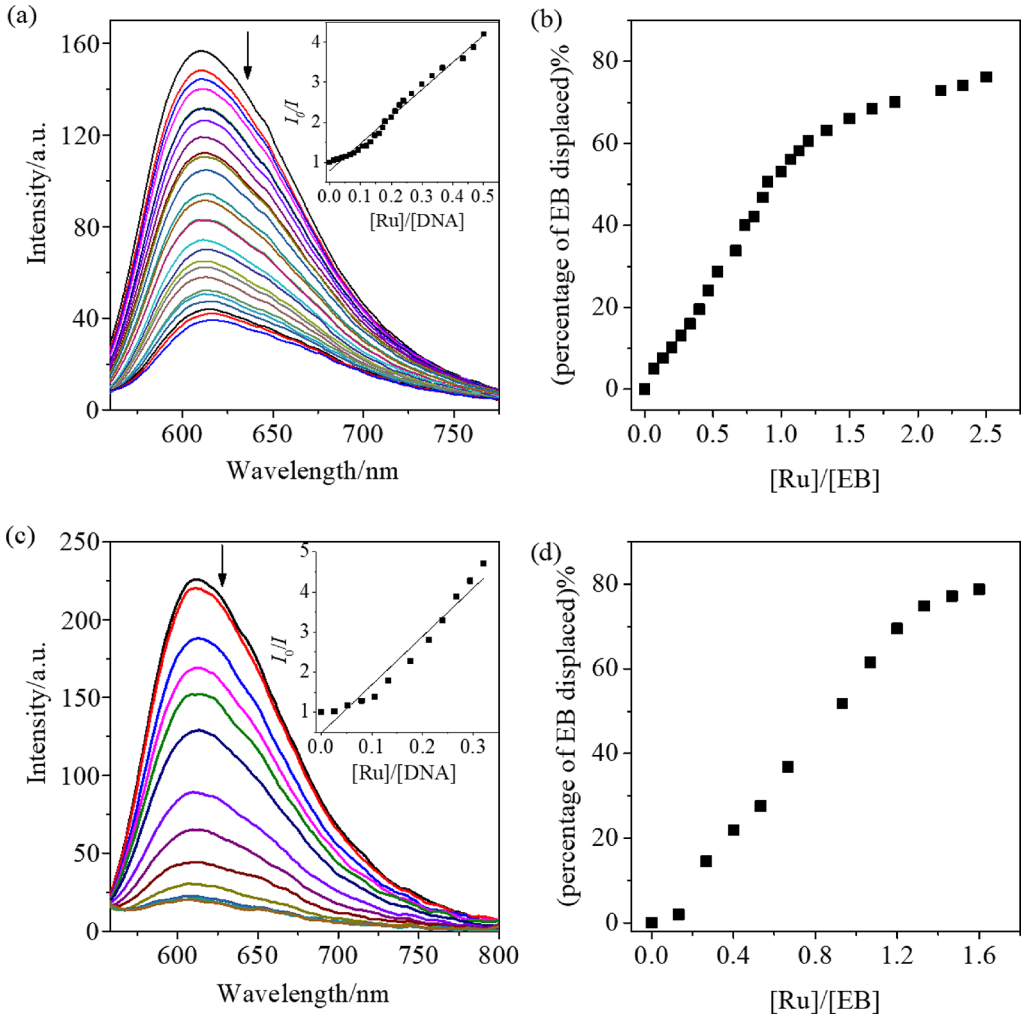

Figure 4. Changes in emission spectra of EB bound to DNA (λ_{ex} = 537 nm) upon increasing concentrations of **Ru1** (0.00−47.62 μM) at [EB] = 20 μM and [DNA] = 100 μM (a) and **Ru2** (0.00−7.94 μM) at [EB] = 5 μM and [DNA] = 25 μM (c). Inset: Stern−Volmer plot of quenching in the emission of DNA-bond EB by the complex. Plot of percentage of EB displaced vs [Ru]/[EB] of **Ru1** (b) and **Ru2** (d).

induced spectral behavior of **Ru2** is in sharp contrast to that of $[Ru(Hpip)_3]^{2+}$ (Hpip = 2-phenylimidazo[4,5-*f*][1,10]-phenanthroline),[78] which showed almost unchanged emission and UV−vis absorption spectral changes during the DNA titrations and was claimed to be a DNA electrostatic binder; the lack of intercalation or groove binding could be understood by the fact that $[Ru(Hpip)_3]^{2+}$ contains three long and large Hpip ligands, which are difficult to accommodate efficiently in the DNA groove, although $[Ru(bpy)_2(Hpip)]^{2+}$ was evidenced to be a DNA intercalator.[79] The aforementioned UV−vis absorption and emission spectral changes induced by binding of the DNA to **Ru1** and **Ru2** provide evidence that electrostatic DNA binding modes of these two complexes could be excluded, but their definite DNA binding modes with respect to intercalation or groove binding need further investigations. It should also be pointed out that the extents of DNA binding induced spectral changes would not always reflect DNA binding affinity, since some very strong DNA binders could result in minor spectral changes.[80]

Competitive Binding to DNA with Ethidium Bromide. To obtain further information on the DNA binding properties of **Ru1** and **Ru2**, a well-established competitive binding experiment was carried out based on the displacement of intercalator EB from a EB-DNA complex.[81] EB is a planar cationic fluorescence dye, and its free state in aqueous solution is very weakly emissive with an emission maximum at 630 nm but displays a dramatic emission enhancement with a hypsochromic shift of 25 nm in the presence of DNA.[43] Addition of a second DNA intercalator was reported to be capable of displacing EB from the EB-ct-DNA complex, and the strong emission from EB-DNA would thus be quenched due to the fact that the excited-state free EB molecules would be readily quenched by the surrounding water molecules.[82]

It can be clearly seen in Figure 4a,c that the emission intensities of the DNA-bound EB appreciably decreased upon the addition of **Ru1** and **Ru2**, indicating a displacement of EB molecules from the EB-ct-DNA complex, and both **Ru1** and **Ru2** acted as DNA intercalators. The quenching plot of I_0/I vs [Ru]/[DNA] (the inset of Figure 4a,c) is in good agreement with the linear Stern−Volmer equation ($I_0/I = 1 + Kr$), and the slopes K are calculated to be 6.76 ± 0.17 and 12.14 ± 0.88 for **Ru1** and **Ru2**, respectively. We also know from these data that 50% of the EB molecules were displaced from DNA-bound EB at concentration ratios $r_{50\%}$ ([Ru]/[EB]) of 0.90 and 0.85 for **Ru1** and **Ru2**, respectively. Furthermore, the values of the apparent DNA binding constant K_{app} of 1.39 × 10^6 M^{-1} for **Ru1** and 1.47 × 10^6 M^{-1} for **Ru2** were derived according to eq

DOI: 10.1021/acs.inorgchem.9b02420
Inorg. Chem. XXXX, XXX, XXX−XXX

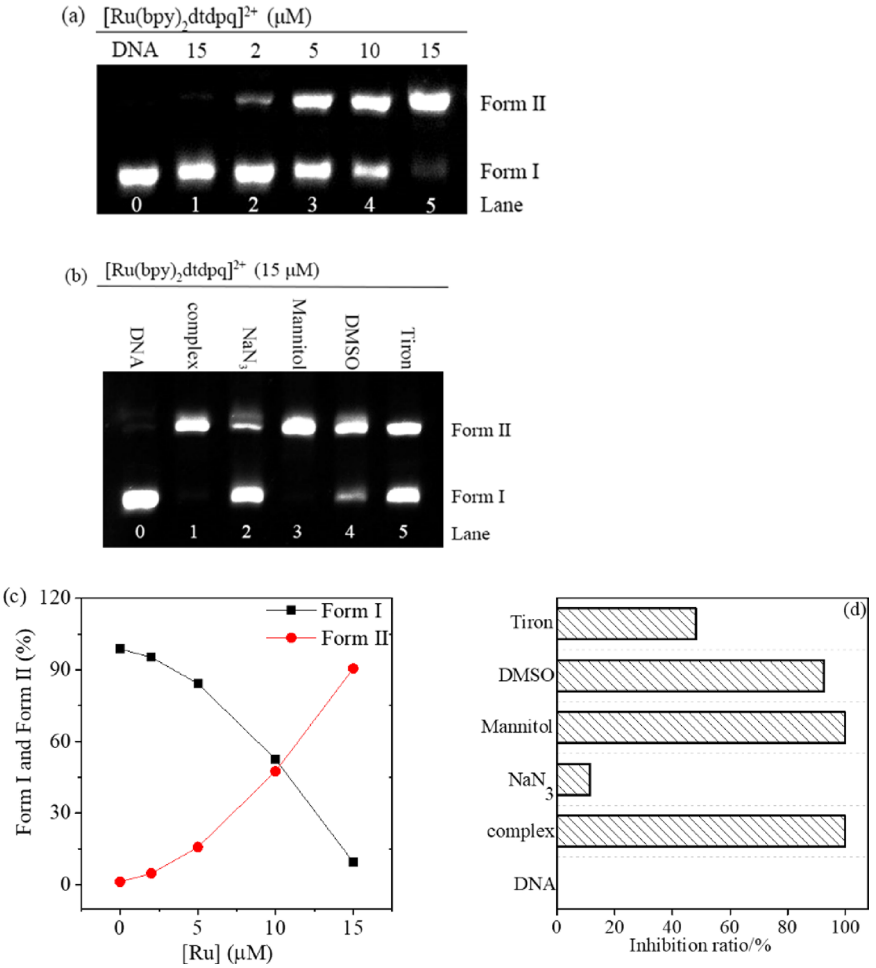

Figure 5. (a) Photocleavage of PUC 18 DNA in the absence (lane 0 with light) and the presence of different concentrations of **Ru1** before (lane 1) and after irradiation (lanes 2−5) 1 h at 360 nm. (b) Photocleavage of PUC 18 DNA by **Ru1** in the absence and presence of different reactive oxygen inhibitors (10 mM Tiron, 200 mM DMSO, 100 mM mannitol, 40 mM NaN_3) upon irradiation for 1 h at 360 nm. (c) Effect of increased concentrations of **Ru1** on the proportions of form I and form II. (d) Bar diagram illustration of the effects of reactive oxygen inhibitors on the DNA photocleavage activity of **Ru1**.

6 by taking a DNA binding constant of 1.25×10^6 M^{-1} for EB:[51]

$$K_{app} = K_b(EB)/r_{50\%} \quad (6)$$

DNA Photocleavage Activity. The DNA photocleavage activities of **Ru1** and **Ru2** were studied by agarose gel electrophoresis. Unfortunately, no related results on **Ru2** were obtained due to its solubility limitation. Interesting DNA photocleavage properties of water-soluble **Ru1** were observed and will be accounted for as follows. The closed-loop supercoil plasmid DNA (form I) is probably scissored to single nicking and/or double nicking to produce relaxed open-circular form II and/or linear form III. When plasmid DNA is subject to electrophoresis, the migration rates follow the decreasing order form I > form III > form II. The DNA photocleavage results are shown in Figure 5a. We observed that no DNA cleavage occurred on control experiments in which the DNA was untreated with **Ru1** (lane 0) and on incubation of plasmid DNA with 15 μM **Ru1** in the dark (lane 1). When plasmid DNA was treated with increasing concentrations of **Ru1** from 2 to 15 μM (lanes 2−5) and was irradiated at 360 nm for 1 h, the amounts of form II increased gradually along with a decrease in form I, suggesting that the DNA cleavage was caused by a photoinduced excited state process of **Ru1** rather than the hydrolytic reaction pathway. As illustrated by the dependence of percentages of forms I and II on the concentrations of **Ru1** (Figure 5c), 91% of the DNA was photocleaved into form II at a **Ru1** concentration of 15 μM.

In order to investigate the DNA photocleavage mechanism of **Ru1**, inhibitions of photocleavage in the presence of different reactive oxygen inhibitors were carried out using NaN_3 as singlet oxygen quenchers, mannitol and DMSO as hydroxyl radical scavengers,[83] and Tiron as a superoxide anion radical scavenger. As shown in Figure 5b,d, the DNA photocleavage was effectively suppressed by NaN_3, with the DNA photocleavage percentage dropping to only 8%, was moderately inhibited by Tiron with 52% photocleavage, and was almost unaffected by mannitol and DMSO, indicating that the DNA photocleavage of **Ru1** could be ascribed to singlet oxygens and superoxide anion radicals generated during the photoinduced processes. This DNA photocleavage behavior is similar to that of $[Ru(bpy)(dppz)(mbpy\text{-}naph)]^{2+}$ (mbpy-naph = 4′-methyl-*N*-(naphthalen-2-yl)-2,2′-bipyridine-4-carboxyamide).[84]

Extracellular Singlet Oxygen Generation. Most studies about $^1O_2$ generation are performed in organic systems, because the $^1O_2$ generated by PSs is easily quenched by

DOI: 10.1021/acs.inorgchem.9b02420
Inorg. Chem. XXXX, XXX, XXX−XXX

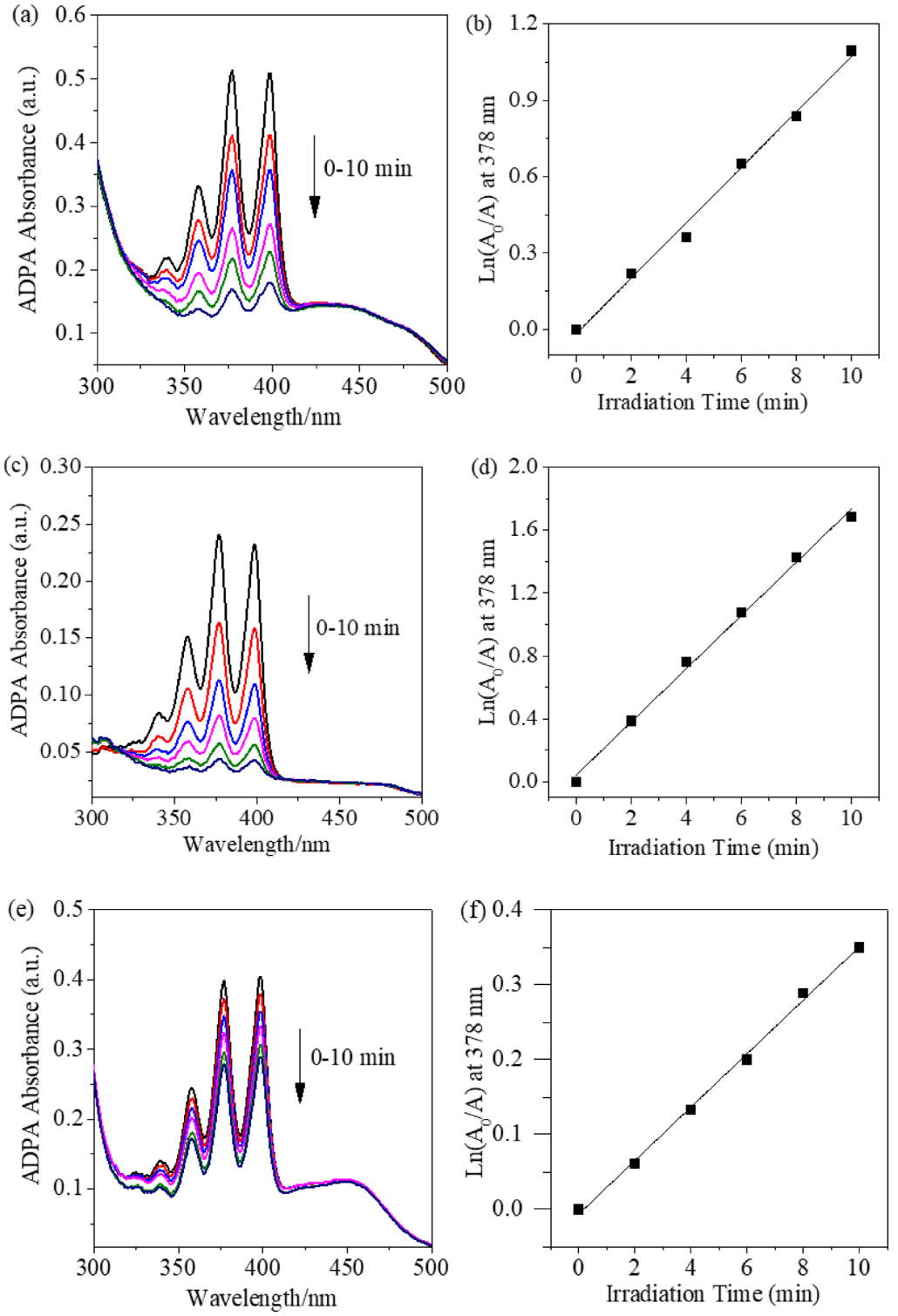

Figure 6. Singlet oxygen generation of ruthenium complexes: (a, c, e) time-dependent absorbance degradation of ADPA mixed with **Ru1**, **Ru2**, and $[Ru(bpy)_2dpq]^{2+}$, respectively, in water under 66 mW/cm^2 visible light irradiation; (b, d, f) plots used for determining photodegradation rate constants of ADPA by light-irradiated **Ru1**, **Ru2** and $[Ru(bpy)_2dpq]^{2+}$, respectively.

surrounding water molecules.[85−87] Herein, the photoinduced production of $^1O_2$ from **Ru1** and **Ru2** in aqueous solutions was confirmed using ADPA as the $^1O_2$ chemical trapping agent. ADPA displays four characteristic bands at 257, 359, 378, and 400 nm. It can irreversibly react with $^1O_2$ produced by photosensitizers, leading to a decrease in characteristic absorption peaks. The absorption spectra of solution mixtures of ADPA and **Ru1** (or **Ru2**) under the irradiation of a 66 mW/cm^2 white light source for 10 min was therefore monitored along with those for the parent complex $[Ru(bpy)_2dpq]^{2+}$ for comparison and were corrected with backgrounds for the respective solutions without ADPA. As shown in Figure 6a,c,e, progressive decreases in the absorption peaks of ADPA with the existence of **Ru1** (3.3 μM), **Ru2** (0.5 μM), and

DOI: 10.1021/acs.inorgchem.9b02420
Inorg. Chem. XXXX, XXX, XXX−XXX

Table 2. IC_{50} (μM) Values for Complex Ru1 in Dark and Light of Different Energy Densities and Comparison with Cisplatin

	IC_{50}[a] (μM)					
	Ru1				cisplatin	
cell line	dark	20 J/cm (PI[b])	30 J/cm (PI[b])	45 J/cm (PI[b])	dark	45 J/cm (PI[b])
HeLa	>100	21.4 ± 1.7 (4.7)	9.6 ± 0.4 (10.4)	6.2 ± 0.3 (16.1)	9.5 ± 0.8	9.1 ± 0.5 (1.0)
A549	>100	8.3 ± 0.4 (12.0)	4.6 ± 0.7 (21.7)	2.1 ± 0.2 (47.6)	18.3 ± 1.2	18.5 ± 0.6 (1.0)
MCF-7	89.39	5.2 ± 0.5 (17.1)	3.1 ± 0.3 (28.8)	2.3 ± 0.3 (38.9)	5.4 ± 0.6	5.8 ± 0.4 (1.0)

[a]The IC_{50} values were determined by an MTT assay after treatment of **Ru1** and cisplatin, and data represent the mean ± SD of at least three independent experiments carried out in triplicate. [b]The phototoxicity index (PI) is the ratio of dark and light IC_{50} values.

$[Ru(bpy)_2dpq]^{2+}$ (3.3 μM) were observed upon irradiation, which suggests that the $^1O_2$ photogenerated by the complexes was trapped by ADPA. By using $^1O_2$ generation rate constant values of 0.11, 0.17, and 0.036 min^{-1} derived from slope values of Figure 6b,d,f, quantum yields for $^1O_2$ generation of **Ru1**, **Ru2**, and $[Ru(bpy)_2dpq]^{2+}$ were derived according to eq 2 using RB as a standard (see Figure S3 in the Supporting Information) to be 18%, 23%, and 6% respectively, indicating that $^1O_2$ generation yields **Ru1** and **Ru2** are much higher than that for the parent complex and even greater than a yield of 10.2% previously reported for $[Ru(bpy)_3]^{2+}$-incorporated UiO-67 metal–organic framework nanoparticles.[50] The results support the fact that the introduction of thiophenyl groups is beneficial for enhancing $^1O_2$ generation. **Ru2**, which has the lowest excited triplet energy among **Ru1**, **Ru2**, and $[Ru(bpy)_2dpq]^{2+}$, exhibited the most rapid generation of $^1O_2$, which is contrast to previous observations on porphyrin-imidazo[4,5-*f*]phenanthroline.[88]

In Vitro Photocytotoxicity. After confirming that **Ru1** could efficiently produce $^1O_2$ upon irradiation, we investigated its photocytotoxicity against the human cervical cancer (HeLa), human lung cancer (A549), and human breast cancer (MCF-7) cell lines. An MTT assay was carried out after treatment with increasing concentrations of **Ru1** at different energy densities of 20, 30, and 45 J/cm^2. The results (see Table 2) demonstrate that the photocytotoxicity of **Ru1** displays concentration-dependent and energy-density-dependent manners. As shown in Figure 7, **Ru1** was almost noncytotoxic against Hela and A549 cell lines (IC_{50} > 100 μM) and had low cytotoxicity against MCF-7 in the dark, while after cells were irradiated with increasing energy densities of 20, 30, and 45 J cm^{-2} which were obtained by systematically adjusting the irradiation time using visible light (25.4 mW/cm^2), significant decreases in cell viabilities were observed. Upon irradiation of 13, 20, or 30 min, the phototoxicity index (PI) values of **Ru1** against A549 cells were measured to be 12.0, 21.7, and 47.6 respectively, which are 2-fold more efficient than those against HeLa cells, which had PI values of 4.7, 10.4, and 16.1 respectively, and similar to the PI values of 17.1, 28.8, and 38.9, respectively, for those against MCF-7 cells. The results indicated that the PDT effects of **Ru1** against A549 cells were higher than those against HeLa cells and were similar to those against MCF-7 cells under the same experimental conditions. In contrast, the IC_{50} values of the clinical drug cisplatin were 9.5 ± 0.8, 18.3 ± 1.2, and 5.4 ± 0.6 μM against HeLa, A549, and MCF-7 cells in dark, respectively, and irradiation had almost negligible effects on cell viability. The photodynamic activity of **Ru2** was not evaluated because of its limited solubility.

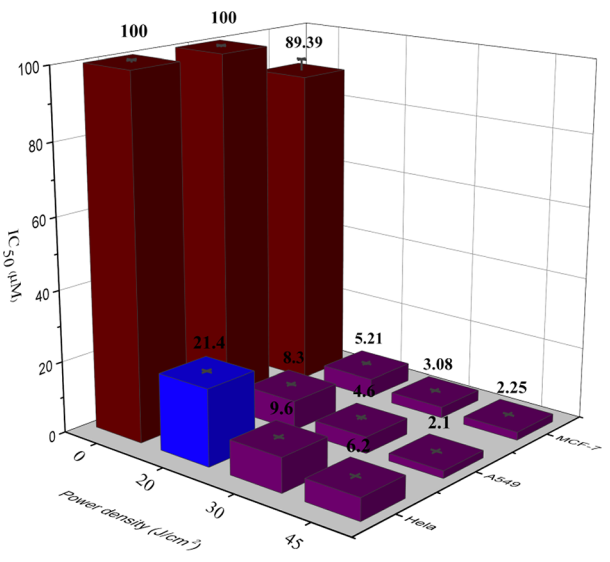

Figure 7. Cytotoxicity against HeLa, A549, and MCF-7 cell lines after treatment with **Ru1** in the absence (dark) and presence (light) of increasing powers of irradiation (20, 30, 45 J cm^{-2}).

In order to explore the process of PDT effects, we continuously observed cell morphological changes for 12 h after irradiating (20 J/cm^2) the **Ru1** (20 μM)-treated cells using ZEISS Celldiscoverer. As shown in Figure S4 (Supporting Information), some cells began to shrink within 4 h of irradiation; when the incubation time was further extended, a large number of cells stopped dividing, indicating that the photoinduced cell apoptosis was caused by **Ru1** after irradiation.

Celluar Uptake. The cellular uptake of PSs is crucial for cellular imaging and PDT treatment efficacy. It was convenient for us to use flow cytometry to study the cellular uptake properties of **Ru1**. First, we determined optimal experimental conditions by checking the quantity of internalized **Ru1** as a function of concentration and incubation time. As shown in Figure S5a,b (Supporting Information), HeLa cells were treated with **Ru1** at different concentrations for 5 h and the emission intensity was measured. In comparison with the control, the emission intensities increased proportionally as the **Ru1** concentrations were increased up to 20 μM; however, the emission intensities no longer increased as the concentrations were further increased. The cytotoxicity assays illustrated that **Ru1** was almost nontoxic against HeLa cells at a concentration of 20 μM; therefore, it is suitable to select 20 μM as the incubating concentration in the following cell imaging study. To investigate the optimal incubation time for cellular uptake of **Ru1**, HeLa cells were treated with **Ru1** for 15 min, 30 min, 1 h, 2 h, 4 h, and 6 h. During the initial incubation period, HeLa cells exhibited a time-dependent uptake of **Ru1**, while cell labeling reached a saturation value after 2 h of incubation, as

DOI: 10.1021/acs.inorgchem.9b02420
Inorg. Chem. XXXX, XXX, XXX−XXX

shown in Figure S5c,d (Supporting Information), which indicated a rapid cellular uptake and excellent cell membrane permeability of **Ru1**. The results demonstrated an optimal concentration of 20 μM and incubation time of 2 h for **Ru1**.

Cellular Localization. The specific accumulation of potential therapeutic and imaging agents in a certain organelle is important to enable their biological activity.[89,90] The emission properties of **Ru1** make it possible to investigate its cellular localization. A cellular uptake study determined by flow cytometry has demonstrated that **Ru1** was effectively internalized into HeLa cells at a high level at the optimal incubation concentration of 20 μM and time of 2 h. In order to further investigate the subcellular localization of **Ru1**, we studied the colocalization behaviors of **Ru1** by codyeing **Ru1** with commercial lysosomal dye (LysoTracker Green) or mitochondrial dye (MitoTracker Green) using confocal microscopy. On the basis of the emission signal distribution of **Ru1** inside of cells, it seemed unlikely to be localized in the nucleus. Colocalization results revealed that the red coloration from **Ru1** did not overlap with the green coloration from the lysosome (Figure 8a). In contrast, as shown in Figure 8b,

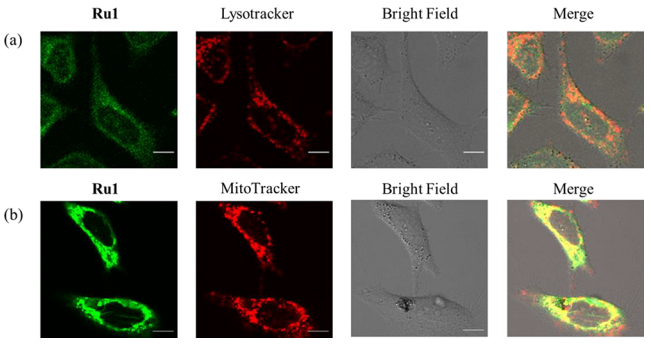

Figure 8. Selective imaging of lysosomes and mitochondria by **Ru1** analyzed by fluorescence confocal microscopy: (a) red and green fluorescence representing the Ru(II) complex and lysosome, respectively; (b) red and green fluorescence representing the Ru(II) complex and mitochondria, respectively. Scale bar: 50 μm.

luminescence images of HeLa cells stained by **Ru1** and MitoTracker Green display a clear regional colocalization (yellow coloration) with a Pearson's colocalization coefficient of 0.73, suggesting that **Ru1** is able to target mitochondria.

Apoptosis Studies. Once cellular apoptosis is initialized, phosphatidylserine is exposed externally to the cell membrane surface because of the loss of asymmetric distribution in the phospholipid bilayer.[91] The exposed phosphatidylserine is a specific molecular target for fluorescently labeled Annexin V-FITC,[92] which could thus be used to identify apoptotic cells. On the other hand, propidium iodide (PI) is able to differentiate viable and necrotic cells.[93] Traditional cell apoptosis analysis commonly uses Annexin V-FITC and PI double labeling measured by flow cytometry, but this well-established double labeling method is unsuitable for the cell apoptosis analysis of **Ru1** in this research because the absorption and emission spectra of **Ru1** and PI are very much overlapped. Therefore, here we used an Annexin V-FITC single-labeling method to detect the apoptosis-inducing ability of **Ru1** upon irradiation and the results are shown in Figure 9. We found that **Ru1** itself at a concentration of 40 μM was not enough to induce cell death in the dark but that irradiation was necessary to trigger cell apoptosis. The percentage of apoptotic cells increased significantly in a **Ru1** concentration dependent manner upon PDT treatment at the same energy density of 20 J/cm^2. When HeLa cells were incubated with **Ru1** at 40 μM for 12 h and then irradiated for 13 min (20 J/cm^2), a total of 82.61% of cells were apoptotic. In comparison with **Ru1**, after identical treatment, the apoptosis-inducing ability of its parent complex $[Ru(bpy)_2dpq]^{2+}$ is much less efficient (17.28%), which may be due to the poor production of $^1O_2$. The above results indicate that the introduction of thiophenyl groups generates excellent PDT effects. Obviously, an energy-density-dependent apoptosis percentage was also observed. When **Ru1** was irradiated with light of varying energy densities of 20, 30, and 45 J/cm^2 at the concentration of 20 μM, the apoptosis percentages were 22.95%, 41.21%, and 96.88%, respectively. The results suggest that the **Ru1** would be a promising PDT agent against cancer.

Detection of Intracellular $^1O_2$ Levels. Singlet oxygen, whether intracellular or extracellular, is capable to trigger apoptosis and regulate programmed cell death.[94] Flow cytometry and inverted fluorescence microscopy were used to analyze the $^1O_2$ levels within HeLa cells photoproduced by **Ru1**. Both techniques are based on the intracellular fluorescence of 2′,7′-dichlorodihydrofluorescein diacetate (H_2DCFDA), which is nonfluorescent but converts to the highly fluorescent 2′,7′-dichlorofluorescein (DCF) after cellular oxidation by $^1O_2$.[91] Detecting the fluorescence intensity of cellular DCF enabled the evaluation of intercellular $^1O_2$ levels. As shown in Figure 10, HeLa cells were pretreated with **Ru1** for 12 h at concentrations of 5, 20, and 40 followed by 13 min of irradiation (20 J/cm^2), and a concentration-dependent fluorescence increase of DCF in HeLa cells was observed. Flow cytometry analysis provided a statistical percentage of cells that were labeled by DCF. After treatment with 40 μM of **Ru1** in combination with light, more than 80% of HeLa cells displayed a high $^1O_2$ level, significantly higher than that with the parent complex ($[Ru(bpy)_2dpq]^{2+}$) (14.66%) under identical experimental conditions. Furthermore, pretreatment of HeLa cells with the $^1O_2$ quencher NaN_3,[95] results in a remarkable inhibition of intracellular $^1O_2$ generation. These results confirm that $^1O_2$ plays a critical role in apoptosis induced by **Ru1**-mediated PDT.

CONCLUSIONS

In conclusion, the thiophenyl-containing dtdpq-based mononuclear mixed-ligand ruthenium(II) complex $[Ru(bpy)_2(dtdpq)](ClO_4)_2$ (**Ru1**) and the homoleptic mononuclear Ru(II) complex $[Ru(dtdpq)_3](ClO_4)_2$ (**Ru2**) have been shown to display extinctly different optical properties; particularly, **Ru2** showed strong solvatochromism with a NIR emission in water peaking at 700 nm, and a 112 nm blue-shifted emission maximum at 588 nm in CH_2Cl_2, which is in sharp contrast to the visible emission maxima of **Ru1** at 600−625 nm in all of the solvents tested with much less sensitive solvatochromism. As revealed by UV−visible absorption and emission titrations, ethidium bromide displacement assay, and agarose gel electrophoresis, **Ru1** and **Ru2** bind intercalatively to ct-DNA with a high affinity of the binding constant on the order of of 10^6 M^{-1}, and **Ru1** at low concentration is capable of photocleaving DNA through singlet oxygen and superoxide anion radical mediated pathway. Under irradiation, **Ru1** and **Ru2** in aqueous solutions display high singlet oxygen generation quantum yields of 18% and 23%, respectively, which are much higher than those of the parent complex

DOI: 10.1021/acs.inorgchem.9b02420
Inorg. Chem. XXXX, XXX, XXX−XXX

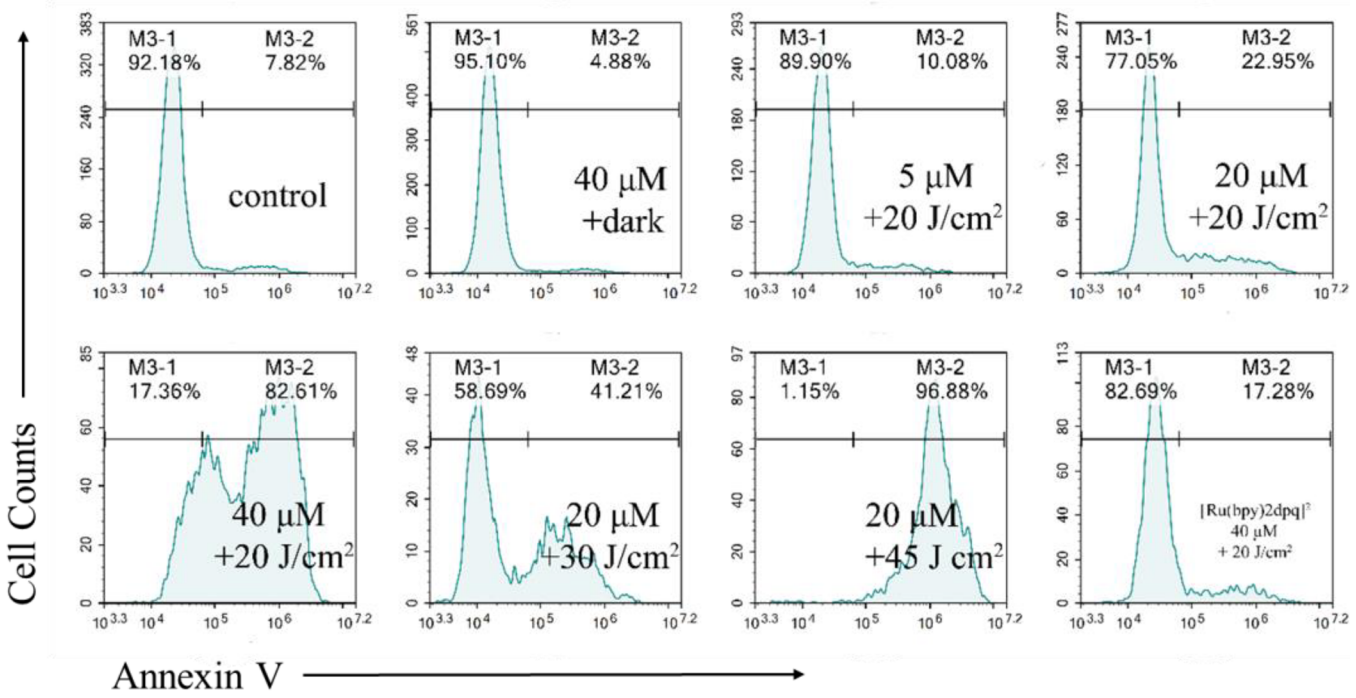

Figure 9. Detection of apoptosis in HeLa cells stained with Annexin V by flow cytometry after **Ru1**-induced PDT treatment at the indicated concentrations.

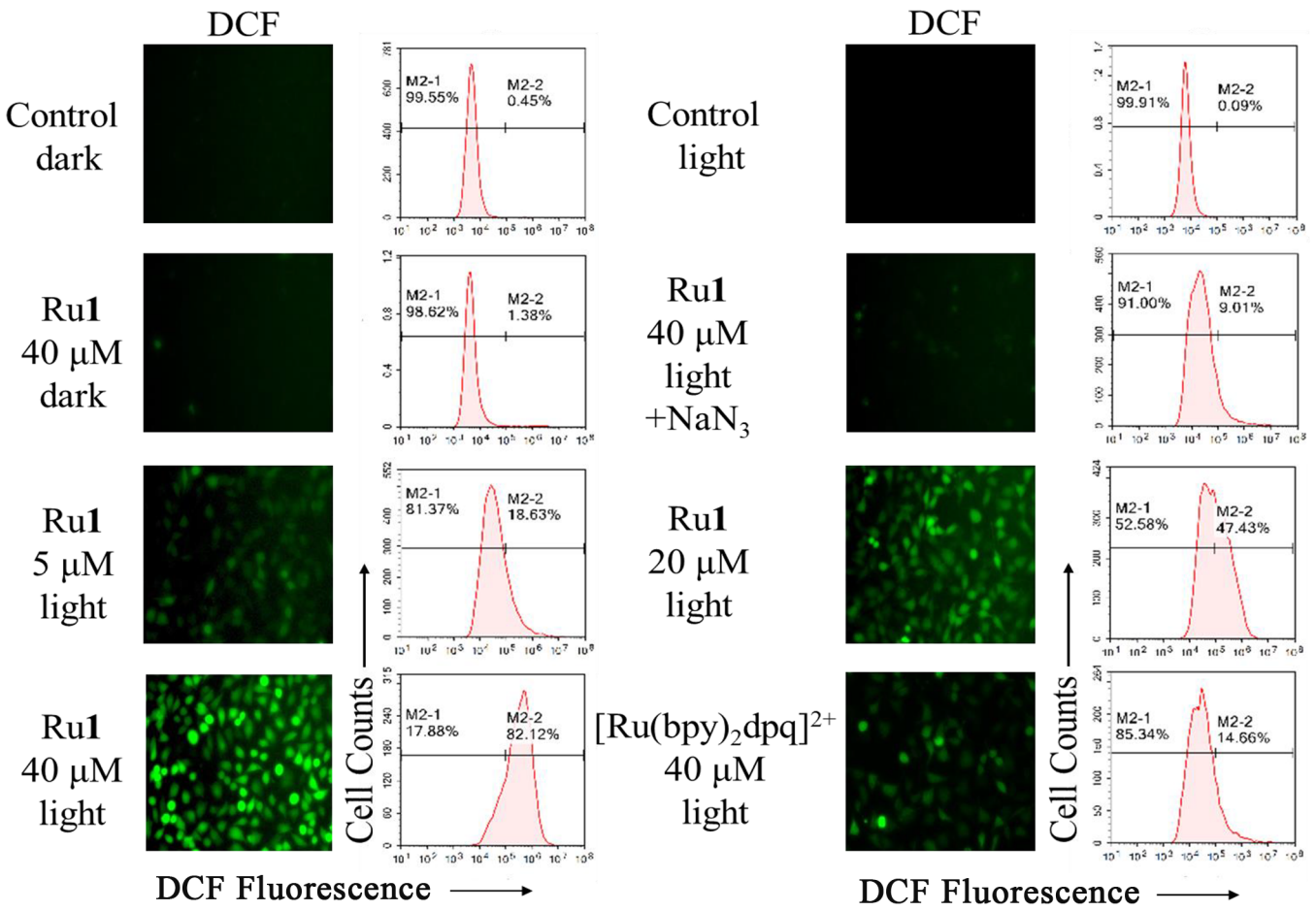

Figure 10. Analysis of $^1O_2$ induced by **Ru1**-mediated PDT using flow cytometry and inverted fluorescence microscopy. HeLa cells were incubated with **Ru1** at the indicated concentrations for 12 h and irradiated with white light for 13 min (20 J/cm^2).

DOI: 10.1021/acs.inorgchem.9b02420
Inorg. Chem. XXXX, XXX, XXX−XXX

($[Ru(bpy)_2dpq]^{2+}$ (6%) and even the $[Ru(bpy)_3]^{2+}$-incorporated UiO-67 metal−organic framework nanoparticles (10.2%) in aqueous solution; the higher singlet oxygen generation ability of **Ru1** in comparison to $[Ru(bpy)_2dpq]^{2+}$ was also demonstrated in HeLa cells. Cellular uptake studies revealed that **Ru1** had good uptake properties and quickly and selectively targeted mitochondria in less than 2 h. PDT experiments showed that **Ru1** is noncytotoxic against HeLa, A549, and MCF-7 cells lines in the dark but exhibited significant PDT effects upon irradiation with visible light (20 J/cm^2) with a maximum PI value of 47.6 toward A549 cells attained. It is verified that the significant PDT effect of **Ru1** originates from its efficient $^1O_2$ generation ability to induce cell apoptosis, and the introduction of thiophenyl groups in **Ru1** is greatly beneficial to the enhancement in PDT effects. Further applications of **Ru1** and molecular modifications on **Ru2** to improve water solubility are being planned.

■ ASSOCIATED CONTENT

Supporting Information

The Supporting Information is available free of charge on the ACS Publications website at DOI: 10.1021/acs.inorgchem.9b02420.

Details of synthesis and characterization, instrumentations and methods for characterization of **Ru1** and **Ru2**, singlet oxygen generation of rose bengal as well as the summary of PDT effect of **Ru1**, and photophysical data of **Ru1** and **Ru2** in different solvents (PDF)

■ AUTHOR INFORMATION

Corresponding Author

*K.-Z.W.: e-mail, kzwang@bnu.edu.cn; fax, +86-10-58802075; tel, +86-10-58805476.

ORCID

Ke-Zhi Wang: 0000-0003-2642-1770

Notes

The authors declare no competing financial interest.

■ ACKNOWLEDGMENTS

This work was supported by the Beijing Municipal Natural Science Foundation (2182028), BNU Interdisciplinary Research Foundation for the First-Year Doctoral Candidates (BNUXKJC1803), National Natural Science Foundation of China (21541010), open grants of Beijing Key Laboratory of Gene Resource and Molecular Development, Analytical and Measurements Fund of Beijing Normal University, and the Doctoral Scientific Research Foundation of Liaoning Province (2019-BS-117).

■ REFERENCES

(1) Qiu, K.; Wang, J.; Song, C.; Wang, L. L.; Zhu, H.; Huang, H.; Huang, J.; Wang, H.; Ji, L. N.; Chao, H. A Crossfire for Two-Photon Photodynamic Therapy with Fluorinated Ruthenium(II) Photosensitizers. *ACS Appl. Mater. Interfaces* **2017**, *9* (22), 18482−18492.

(2) Jemal, A.; Center, M. M.; Desantis, C.; Ward, E. M. Global patterns of cancer incidence and mortality rates and trends. *Cancer Epidemiol., Biomarkers Prev.* **2010**, *19* (8), 1893−1907.

(3) Singha, K.; Laha, P.; Chandra, F.; Dehury, N.; Koner, A. L.; Patra, S. Long-Lived Polypyridyl Based Mononuclear Ruthenium Complexes: Synthesis, Structure, and Azo Dye Decomposition. *Inorg. Chem.* **2017**, *56* (11), 6489−6498.

(4) Zheng, Y.; He, L.; Zhang, D. Y.; Tan, C. P.; Ji, L. N.; Mao, Z. W. Mixed-ligand iridium(III) complexes as photodynamic anticancer agents. *Dalton Trans* **2017**, *46* (34), 11395−11407.

(5) Martinez, M. A.; Carranza, M. P.; Massaguer, A.; Santos, L.; Organero, J. A.; Aliende, C.; de Llorens, R.; Ng-Choi, I.; Feliu, L.; Planas, M.; Rodriguez, A. M.; Manzano, B. R.; Espino, G.; Jalón, F. A. Synthesis and Biological Evaluation of Ru(II) and Pt(II) Complexes Bearing Carboxyl Groups as Potential Anticancer Targeted Drugs. *Inorg. Chem.* **2017**, *56* (22), 13679−13696.

(6) Rohrabaugh, T. N.; Collins, K. A.; Xue, C.; White, J. K.; Kodanko, J. J.; Turro, C. New Ru (II) complex for dual photochemotherapy: release of cathepsin K inhibitor and $_1O^2$ production. *Dalton Trans* **2018**, *47* (34), 11851−11858.

(7) Arora, K.; Herroon, M.; Al-Afyouni, M. H.; Toupin, N. P.; Rohrabaugh, T. N., Jr.; Loftus, L. M.; Podgorski, I.; Turro, C.; Kodanko, J. J. Catch and Release Photosensitizers: Combining Dual-Action Ruthenium Complexes with Protease Inactivation for Targeting Invasive Cancers. *J. Am. Chem. Soc.* **2018**, *140* (43), 14367−14380.

(8) Zhang, D. Y.; Zheng, Y.; Tan, C. P.; Sun, J. H.; Zhang, W.; Ji, L. N.; Mao, Z. W. Graphene oxide decorated with Ru (II)−polyethylene glycol complex for lysosome-targeted imaging and photodynamic/photothermal therapy. *ACS Appl. Mater. Interfaces* **2017**, *9* (8), 6761−6771.

(9) Tian, N.; Sun, W.; Guo, X.; Lu, J.; Li, C.; Hou, Y.; Wang, X.; Zhou, Q. Mitochondria targeted and NADH triggered photodynamic activity of chloromethyl modified Ru(II) complexes under hypoxic conditions. *Chem. Commun.* **2019**, *55* (18), 2676−2679.

(10) Jakubaszek, M.; Goud, B.; Ferrari, S.; Gasser, G. Mechanisms of action of Ru(II) polypyridyl complexes in living cells upon light irradiation. *Chem. Commun.* **2018**, *54* (93), 13040−13059.

(11) Poulsen, B. C.; Estalayo-Adrian, S.; Blasco, S.; Bright, S. A.; Kelly, J. M.; Williams, D. C.; Gunnlaugsson, T. Luminescent ruthenium polypyridyl complexes with extended 'dppz' like ligands as DNA targeting binders and cellular agents. *Dalton Trans* **2016**, *45* (45), 18208−18220.

(12) Simplicio, F. I.; Maionchi, F.; Hioka, N. Photodynamic therapy: pharmacological aspects, applications and recent advances in drug development. *Quim. Nova* **2002**, *25* (5), 801−807.

(13) Ochsner, M. Photophysical and photobiological processes in the photodynamic therapy of tumors. *J. Photochem. Photobiol., B* **1997**, *39* (1), 1−18.

(14) Aksakal, N. E.; Kazan, H. H.; Ecik, E. T.; Yuksel, F. A novel photosensitizer based on a ruthenium(II) phenanthroline bis-(perylenediimide) dyad: synthesis, generation of singlet oxygen and in vitro photodynamic therapy. *New J. Chem.* **2018**, *42* (21), 17538−17545.

(15) Monro, S.; Colon, K. L.; Yin, H.; Roque, J.; Konda, P.; Gujar, S.; Thummel, R. P.; Lilge, L.; Cameron, C. G.; McFarland, S. A. Transition Metal Complexes and Photodynamic Therapy from a Tumor-Centered Approach: Challenges, Opportunities, and Highlights from the Development of TLD1433. *Chem. Rev.* **2019**, *119* (2), 797−828.

(16) Kaspler, P.; Lazic, S.; Forward, S.; Arenas, Y.; Mandel, A.; Lilge, L. A ruthenium(II) based photosensitizer and transferrin complexes enhance photo-physical properties, cell uptake, and photodynamic therapy safety and efficacy. *Photochem. Photobiol. Sci.* **2016**, *15* (4), 481−495.

(17) Ghosh, G.; Colón, K. L.; Fuller, A.; Sainuddin, T.; Bradner, E.; McCain, J.; Monro, S. M.; Yin, H.; Hetu, M. W.; Cameron, C. G. Cyclometalated Ruthenium (II) Complexes Derived from α-Oligothiophenes as Highly Selective Cytotoxic or Photocytotoxic Agents. *Inorg. Chem.* **2018**, *57* (13), 7694−7712.

(18) Sainuddin, T.; Pinto, M.; Yin, H.; Hetu, M.; Colpitts, J.; McFarland, S. A. Strained ruthenium metal−organic dyads as photocisplatin agents with dual action. *J. Inorg. Biochem.* **2016**, *158*, 45−54.

DOI: 10.1021/acs.inorgchem.9b02420
Inorg. Chem. XXXX, XXX, XXX−XXX

(19) Alberto, M. E.; Pirillo, J.; Russo, N.; Adamo, C. Theoretical exploration of type I/type II dual photoreactivity of promising Ru (II) dyads for PDT approach. *Inorg. Chem.* **2016**, *55* (21), 11185−11192.
(20) Shi, G.; Monro, S.; Hennigar, R.; Colpitts, J.; Fong, J.; Kasimova, K.; Yin, H.; DeCoste, R.; Spencer, C.; Chamberlain, L. Ru(II) dyads derived from α-oligothiophenes: A new class of potent and versatile photosensitizers for PDT. *Coord. Chem. Rev.* **2015**, *282-283*, 127−138.
(21) Li, Z. S.; Yang, H. X.; Zhang, A. G.; Luo, H.; Wang, K. Z. pH effects on optical and DNA binding properties of a thiophene-containing ruthenium(II) complex. *Inorg. Chim. Acta* **2011**, *370* (1), 132−140.
(22) Yuan, C. L.; Zhang, A. G.; Zheng, Z. B.; Wang, K. Z. The effects of structural variations of thiophene-containing Ru(II) complexes on the acid−base and DNA binding properties. *J. Biomol. Struct. Dyn.* **2013**, *31* (3), 316−330.
(23) Zhao, X. L.; Li, Z. S.; Zheng, Z. B.; Zhang, A. G.; Wang, K. Z. pH luminescence switch, DNA binding and photocleavage, and cytotoxicity of a dinuclear ruthenium complex. *Dalton Trans* **2013**, *42* (16), 5764−5777.
(24) Zhao, X. L.; Li, Z. S.; Zhang, A. G.; Liu, P.; Song, X. M.; Wang, K. Z. pH and DNA luminescence switching, DNA photocleavage and cytotoxic properties of two thiophene-containing ruthenium(II) complexes. *Eur. J. Med. Chem.* **2014**, *87*, 10−22.
(25) Chaves, N. L.; Lopes, C. A. P.; Carneiro, M. L. B.; Ribeiro de Souza, A.; Oliveira da Silva, M.; Correa, J. R.; Bao, S. N. Rhodium citrate associated with maghemite nanoparticles causes DNA fragmentation independently of caspases 3 and mediated by reactive oxygen species. *J. Nanomed. Nanotechnol.* **2015**, *6* (5), 1000312.
(26) Gill, M. R.; Jarman, P. J.; Halder, S.; Walker, M. G.; Saeed, H. K.; Thomas, J. A.; Smythe, C.; Ramadan, K.; Vallis, K. A. A three-in-one-bullet for oesophageal cancer: replication fork collapse, spindle attachment failure and enhanced radiosensitivity generated by a ruthenium(II) metallo-intercalator. *Chem. Sci.* **2018**, *9* (4), 841−849.
(27) Zhang, H. Z.; He, S. C.; Peng, Y. J.; Zhang, H. J.; Gopala, L.; Tangadanchu, V. K. R.; Gan, L. L.; Zhou, C. H. Design, synthesis and antimicrobial evaluation of novel benzimidazole-incorporated sulfonamide analogues. *Eur. J. Med. Chem.* **2017**, *136*, 165−183.
(28) Cheng, N.; Chen, Y.; Yu, J.; Li, J.-j.; Liu, Y. Enhanced DNA binding and photocleavage abilities of β-cyclodextrin appended Ru(II) complex through supramolecular strategy. *Bioconjugate Chem.* **2018**, *29* (6), 1829−1833.
(29) Sun, B.; Liang, Z.; Xie, B. P.; Li, R.-T.; Li, L. Z.; Jiang, Z. H.; Bai, L. P.; Chen, J. X. Fluorescence sensing platform based on ruthenium(II) complexes as high 3S (sensitivity, specificity, speed) and "on-off-on" sensors for the miR-185 detection. *Talanta* **2018**, *179*, 658−667.
(30) Boynton, A. N.; Marcelis, L.; McConnell, A. J.; Barton, J. K. A ruthenium(II) complex as a luminescent probe for DNA mismatches and abasic sites. *Inorg. Chem.* **2017**, *56* (14), 8381−8389.
(31) Yu, H. J.; Hao, Z. F.; Peng, H.l.; Rao, R. H.; Sun, M.; Ross, A. W.; Ran, C.; Chao, H.; Yu, L. Near-infrared lysosome pH tracker and naked-eye colorimetric nucleic acids sensor based on ruthenium complexes $[Ru(bim)_2(dppz)]^{2+}$ and $[Ru(bim)_2(pip)]^{2+}$. *Sens. Actuators, B* **2017**, *252*, 313−321.
(32) Friedman, A. E.; Chambron, J. C.; Sauvage, J. P.; Turro, N. J.; Barton, J. K. A molecular light switch for DNA: $Ru(bpy)_2(dppz)^{2+}$. *J. Am. Chem. Soc.* **1990**, *112* (39), 4960−4962.
(33) Wang, F.; Ma, S.; Feng, Y.; Liu, X.; Tan, L. Binding properties of two Ru(II) polypyridyl complexes containing dppz units and fluorine groups with poly(U)·poly(A)*poly(U) triplex. *J. Inorg. Biochem.* **2019**, *197*, 110705.
(34) Fairbanks, S. D.; Robertson, C. C.; Keene, F. R.; Thomas, J. A.; Williamson, M. P. Structural investigation into the threading intercalation of a chiral dinuclear ruthenium (II) polypyridyl complex through a B-DNA oligonucleotide. *J. Am. Chem. Soc.* **2019**, *141* (11), 4644−4652.
(35) Mårtensson, A. K.; Lincoln, P. Effects of methyl substitution on DNA binding enthalpies of enantiopure $Ru(phenanthroline)_2$ dipyridophenazine^{2+} complexes. *Phys. Chem. Chem. Phys.* **2018**, *20* (16), 11336−11341.
(36) Bhat, S. S.; Revankar, V. K.; Pinjari, R. V.; Naveen, S.; Bogar, C.; Bhat, K.; Kawade, V. A. Efficient DNA condensation by ruthenium(II) polypyridyl complexes containing triptycenyl functionalized 1, 10-phenanthroline. *New J. Chem.* **2017**, *41* (13), 5513−5520.
(37) Delaney, S.; Pascaly, M.; Bhattacharya, P. K.; Han, K.; Barton, J. K. Oxidative damage by ruthenium complexes containing the dipyridophenazine ligand or its derivatives: a focus on intercalation. *Inorg. Chem.* **2002**, *41* (7), 1966−1974.
(38) Aldrich-Wright, J. R.; Greguric, I.; Vagg, R. S.; Vickery, K.; Williams, P. A. Development of DNA-immobilized chromatographic stationary phases for optical resolution and DNA-affinity comparison of metal complexes. *J. Chromatogr. A* **1995**, *718* (2), 436−43.
(39) O'Donoghue, K. A.; Kelly, J. M.; Kruger, P. E. Unusual photophysical switching in a Ru(II) diimine DNA probe caused by amide functionalisation. *Dalton Trans* **2004**, No. 1, 13−15.
(40) Collins, J. G.; Sleeman, A. D.; Aldrich-Wright, J. R.; Greguric, I.; Hambley, T. W. A ^{1}H NMR study of the DNA binding of ruthenium (II) polypyridyl complexes. *Inorg. Chem.* **1998**, *37* (13), 3133−3141.
(41) O'Donoghue, K.; Penedo, J. C.; Kelly, J. M.; Kruger, P. E. Photophysical study of a family of $[Ru(phen)_2(Mendpq)]^{2+}$ complexes in different solvents and DNA: a specific water effect promoted by methyl substitution. *Dalton Trans* **2005**, *6* (6), 1123−1128.
(42) Ambroise, A.; Maiya, B. G. Ruthenium(II) Complexes of 6,7-Dicyanodipyridoquinoxaline: Synthesis, Luminescence Studies, and DNA Interaction. *Inorg. Chem.* **2000**, *39* (19), 4264−72.
(43) Zhang, A. G.; Zhang, Y. Z.; Duan, Z. M.; Wang, K. Z.; We, H. B.; Bian, Z. Q.; Huang, C. H. Dual molecular light switches for pH and DNA based on a novel Ru(II) complex. A non-intercalating Ru(II) complex for DNA molecular light switch. *Inorg. Chem.* **2011**, *50* (14), 6425−6436.
(44) Han, M. J.; Duan, Z. M.; Hao, Q.; Shuaizhi Zheng, A.; Wang, K. Z. Molecular Light Switches for Calf Thymus DNA Based on Three Ru(II) Bipyridyl Complexes with Variations of Heteroatoms. *J. Phys. Chem. C* **2007**, *111* (44), 16577−16585.
(45) Alessio, E.; Mestroni, G.; Bergamo, A.; Sava, G. Ruthenium antimetastatic agents. *Curr. Top. Med. Chem.* **2004**, *4* (15), 1525−1535.
(46) Yao, C. J.; Zhong, Y. W.; Nie, H. J.; Abruna, H. D.; Yao, J. Near-IR Electrochromism in Electropolymerized Films of a Biscyclometalated Ruthenium Complex Bridged by 1,2,4,5-Tetra(2-pyridyl)benzene. *J. Am. Chem. Soc.* **2011**, *133* (51), 20720−20723.
(47) Liu, J. G.; Zhang, Q. L.; Shi, X. F.; Ji, L. N. Interaction of $Ru(dmp)_2(dppz)^{2+}$ and $Ru(dmb)_2(dppz)^{2+}$ with DNA: Effects of the ancillary ligands on the DNA-binding behaviors. *Inorg. Chem.* **2001**, *40* (19), 5045−5050.
(48) Azar, D. F.; Audi, H.; Farhat, S.; El-Sibai, M.; Abi-Habib, R. J.; Khnayzer, R. S. Phototoxicity of strained Ru(II) complexes: is it the metal complex or the dissociating ligand? *Dalton Trans* **2017**, *46* (35), 11529−11532.
(49) Martin, A.; Byrne, A.; Burke, C. S.; Forster, R. J.; Keyes, T. E. Peptide-Bridged Dinuclear Ru(II) Complex for Mitochondrial Targeted Monitoring of Dynamic Changes to Oxygen Concentration and ROS Generation in Live Mammalian Cells. *J. Am. Chem. Soc.* **2014**, *136* (43), 15300−15309.
(50) Chen, R.; Zhang, J.; Chelora, J.; Xiong, Y.; Kershaw, S. V.; Li, K. F.; Lo, P. K.; Cheah, K. W.; Rogach, A. L.; Zapien, J. A. Ruthenium (II) Complex Incorporated UiO-67 Metal-Organic Frameworks Nanoparticles for Enhanced Two-Photon Fluorescence Imaging and Photodynamic Cancer Therapy. *ACS Appl. Mater. Interfaces* **2017**, *9* (7), 5699−5708.
(51) Saha, D.; Das, S.; Karmakar, S.; Dutta, S.; Baitalik, S. Synthesis, structural characterization and anion-, cation- and solvent-induced tuning of photophysical properties of a bimetallic Ru(II) complex: combined experimental and DFT/TDDFT investigation. *RSC Adv.* **2013**, *3* (38), 17314−17334.

DOI: 10.1021/acs.inorgchem.9b02420
Inorg. Chem. XXXX, XXX, XXX−XXX

(52) Ielasi, G.; Alcover, G.; Casellas, J.; de Graaf, C.; Orellana, G.; Reguero, M. Computer-aided design of short-lived phosphorescent Ru(II) polarity probes. *Dyes Pigm.* **2019**, *162*, 168−176.
(53) Lolage, S. R.; Pawal, S. B.; Chavan, S. S. Heterobimetallic Cu(I)/Ru(II) Acetylide Bridged Hybrid Complexes Containing Coordination and Organometallic Sites. *ChemistrySelect* **2017**, *2* (26), 8052−8058.
(54) Leung, M. Y.; Leung, S. Y.L.; Wu, D.; Yu, T.; Yam, V. W.W. Synthesis, Electrochemistry, and Photophysical Studies of Ruthenium-(II) Polypyridine Complexes with D-π-A-π-D Type Ligands and Their Application Studies as Organic Memories. *Chem. - Eur. J.* **2016**, *22* (39), 14013−14021.
(55) Xiang, H.; Cheng, J.; Ma, X.; Zhou, X.; Chruma, J. J. Near-Infrared Phosphorescence: Materials and Applications. *Chem. Soc. Rev.* **2013**, *42* (14), 6128−6185.
(56) Meng, T. T.; Wang, H.; Zheng, Z. B.; Wang, K. Z. pH-Switchable "Off−On−Off" Near-Infrared Luminescence Based on a Dinuclear Ruthenium(II) Complex. *Inorg. Chem.* **2017**, *56* (9), 4775−4779.
(57) Schulze, M.; Steffen, A.; Würthner, F. Near-IR Phosphorescent Ruthenium(II) and Iridium(III) Perylene Bisimide Metal Complexes. *Angew. Chem., Int. Ed.* **2015**, *54* (5), 1570−1573.
(58) Chen, J. L.; Chi, Y.; Chen, K.; Cheng, Y. M.; Chung, M. W.; Yu, Y. C.; Lee, G. H.; Chou, P. T.; Shu, C. F. New series of ruthenium(II) and osmium(II) complexes showing solid-state phosphorescence in far-visible and near-infrared. *Inorg. Chem.* **2010**, *49* (3), 823−32.
(59) Xun, S.; Zhang, J.; Li, X.; Ma, D.; Zhi, Y. W. Synthesis and near-infrared luminescent properties of some ruthenium complexes. *Synth. Met.* **2008**, *158* (12), 484−488.
(60) Liu, X. W.; Li, J.; Hong, D.; Zheng, K. C.; Mao, Z. W.; Ji, L. N. Experimental and DFT studies on the DNA-binding trend and spectral properties of complexes $[Ru(bpy)_2L]^{2+}$ (L = dmdpq, dpq, and dcdpq). *Inorg. Chim. Acta* **2005**, *358* (12), 3311−3319.
(61) Chen, Y. M.; Liu, Y. J.; Li, Q.; Wang, K. Z. pH-and DNA-induced dual molecular light switches based on a novel ruthenium (II) complex. *J. Inorg. Biochem.* **2009**, *103* (10), 1395−1404.
(62) Chen, X.; Gao, F.; Yang, W. Y.; Sun, J.; Zhou, Z. X.; Ji, L. N. Effects of intercalative ligands on the DNA binding, DNA topoisomerase II and DNA transcription inhibition of polypyridyl ruthenium(II) complexes. *Inorg. Chim. Acta* **2011**, *378* (1), 140−147.
(63) Tripathy, S. K.; De, U.; Dehury, N.; Laha, P.; Panda, M. K.; Kim, H. S.; Patra, S. Cyclometallated iridium complexes inducing paraptotic cell death like natural products: synthesis, structure and mechanistic aspects. *Dalton Trans* **2016**, *45* (38), 15122−15136.
(64) Gao, F.; Chen, X.; Wang, J. Q.; Chen, Y.; Chao, H.; Ji, L. N. In vitro transcription inhibition by ruthenium(II) polypyridyl complexes with electropositive ancillary ligands. *Inorg. Chem.* **2009**, *48* (13), 5599−5601.
(65) Zhen, Q.-X.; Ye, B.-H.; Zhang, Q.-L.; Liu, J.-G.; Hong Li; Ji, L.-N.; Wang, L. Synthesis, characterization and the effect of ligand planarity of $[Ru(bpy)_2L]^{2+}$ on DNA binding affinity. *J. Inorg. Biochem.* **1999**, *76* (1), 47−53.
(66) O'Donoghue, K. A.; Kelly, J. M.; Kruger, P. E. Unusual photophysical switching in a Ru(II) diimine DNA probe caused by amide functionalisation. *Dalton Trans* **2004**, *1* (1), 13−15.
(67) Han, M. J.; Duan, Z. M.; Hao, Q.; Zheng, S. Z.; Wang, K. Z. Molecular Light Switches for Calf Thymus DNA Based on Three Ru(II) Bipyridyl Complexes with Variations of Heteroatoms. *J. Phys. Chem. C* **2007**, *111* (44), 16577−16585.
(68) Barton, J. Metals and DNA: molecular left-handed complements. *Science* **1986**, *233* (4765), 727−734.
(69) Mariappan, M.; Maiya, B. G. Effects of Anthracene and Pyrene Units on the Interactions of Novel Polypyridylruthenium(II) Mixed-Ligand Complexes with DNA. *Eur. J. Inorg. Chem.* **2005**, *2005* (11), 2164−2173.
(70) Brennaman, M. K.; Meyer, T. J.; Papanikolas, J. M. $[Ru(bpy)_2dppz]^{2+}$ Light-Switch Mechanism in Protic Solvents as Studied through Temperature-Dependent Lifetime Measurements. *J. Phys. Chem. A* **2004**, *108* (45), 9938−9944.
(71) Han, M. J.; Chen, Y. M.; Wang, K. Z. Ruthenium(II) complexes of 6-hydroxyl-dipyrido[3,2-a:2′,3′-c]phenazine: self association, and concentration-dependent acid-base and DNA-binding properties. *New J. Chem.* **2008**, *32* (6), 970−980.
(72) Elmes, R. B. P.; Kitchen, J. A.; Williams, D. C.; Gunnlaugsson, T. Pushing the limit: synthesis, photophysical and DNA binding studies of a NIR-emitting Ru(II)-polypyridyl probe with 'light switch' behaviour. *Dalton Trans* **2012**, *41* (22), 6607−6610.
(73) Mardanya, S.; Mondal, D.; Baitalik, S. Bimetallic Ru(II) and Os(II) complexes based on a pyrene-bisimidazole spacer: synthesis, photophysics, electrochemistry and multisignalling DNA binding studies in the near infrared region. *Dalton Trans* **2017**, *46* (48), 17010−17024.
(74) Mardanya, S.; Karmakar, S.; Mondal, D.; Baitalik, S. Homo- and Heterobimetallic Ruthenium(II) and Osmium(II) Complexes Based on a Pyrene-Biimidazolate Spacer as Efficient DNA-Binding Probes in the Near-Infrared Domain. *Inorg. Chem.* **2016**, *55* (7), 3475−3489.
(75) Brabec, V.; Kasparkova, J. Ruthenium coordination compounds of biological and biomedical significance. DNA binding agents. *Coord. Chem. Rev.* **2018**, *376*, 75−94.
(76) Gill, M. R.; Thomas, J. A. Ruthenium (II) polypyridyl complexes and DNA—from structural probes to cellular imaging and therapeutics. *Chem. Soc. Rev.* **2012**, *41* (8), 3179−3192.
(77) Komor, A. C.; Barton, J. K. The path for metal complexes to a DNA target. *Chem. Commun.* **2013**, *49* (35), 3617−3630.
(78) Wu, J. Z.; Ji, L. N. Synthesis and spectroscopic DNA binding studies of homoleptic and heteroleptic ruthenium (II) complexes with imidazo [4,5-f][1,10] phenanthroline or its derivatives. *Transition Met. Chem.* **1999**, *24* (3), 299−303.
(79) Wu, J. Z.; Ye, B. H.; Wang, L.; Ji, L. N.; Zhou, J. Y.; Li, R. H.; Zhou, Z. Y. Bis (2, 2′-bipyridine) ruthenium (II) complexes with imidazo [4,5-f][1,10]-phenanthroline or 2-phenylimidazo [4,5-*f*]-[1,10] phenanthroline. *J. Chem. Soc., Dalton Trans.* **1997**, No. 8, 1395−1402.
(80) Ju, C. C.; Zhang, A. G.; Yuan, C. L.; Zhao, X. L.; Wang, K. Z. The interesting DNA-binding properties of three novel dinuclear Ru(II) complexes with varied lengths of flexible bridges. *J. Inorg. Biochem.* **2011**, *105* (3), 435−443.
(81) Gupta, R. K.; Kumar, A.; Paitandi, R. P.; Singh, R. S.; Mukhopadhyay, S.; Verma, S. P.; Das, P.; Pandey, D. S. Heteroleptic arene Ru(II) dipyrrinato complexes: DNA, protein binding and anti-cancer activity against the ACHN cancer cell line. *Dalton Trans* **2016**, *45* (16), 7163−7177.
(82) Khan, N. H.; Pandya, N.; Kureshy, R. I.; Abdi, S. H. R.; Agrawal, S.; Bajaj, H. C.; Pandya, J.; Gupte, A. Synthesis, characterization, DNA binding and cleavage studies of chiral Ru(II) salen complexes. *Spectrochim. Acta, Part A* **2009**, *74* (1), 113−119.
(83) Ghosh, A.; Mandoli, A.; Kumar, D. K.; Yadav, N. S.; Ghosh, T.; Jha, B.; Thomas, J. A.; Das, A. DNA binding and cleavage properties of a newly synthesised Ru(II)-polypyridyl complex. *Dalton Trans* **2009**, No. 42, 9312−9321.
(84) Abreu, F. D. G.; Paulo, T. d. F.; Gehlen, M. H.; Ando, R. M. A.; Lopes, L. G.; Gondim, A. C. U. S.; Vasconcelos, M. A.; Teixeira, E. H.; Sousa, E. H. S.; de Carvalho, I. M. M. Aryl-substituted ruthenium (II) complexes: A strategy for enhanced photocleavage and efficient DNA binding. *Inorg. Chem.* **2017**, *56* (15), 9084−9096.
(85) Raza, M. K.; Gautam, S.; Howlader, P.; Bhattacharyya, A.; Kondaiah, P.; Chakravarty, A. R. Pyriplatin-Boron-Dipyrromethene Conjugates for Imaging and Mitochondria-Targeted Photodynamic Therapy. *Inorg. Chem.* **2018**, *57* (22), 14374−14385.
(86) Kim, Y.; Koo, J.; Hwang, I.-C.; Mukhopadhyay, R. D.; Hong, S.; Yoo, J.; Dar, A. A.; Kim, I.; Moon, D.; Shin, T. J.; Ko, Y. H.; Kim, K. Rational Design and Construction of Hierarchical Superstructures Using Shape-Persistent Organic Cages: Porphyrin Box-Based Metallosupramolecular Assemblies. *J. Am. Chem. Soc.* **2018**, *140* (44), 14547−14551.
(87) Ramu, V.; Gautam, S.; Garai, A.; Kondaiah, P.; Chakravarty, A. R. Glucose-Appended Platinum(II)-BODIPY Conjugates for Tar-

DOI: 10.1021/acs.inorgchem.9b02420
Inorg. Chem. XXXX, XXX, XXX−XXX

geted Photodynamic Therapy in Red Light. *Inorg. Chem.* **2018**, *57* (4), 1717−1726.
(88) Jiang, J.; Liu, D.; Zhao, Y.; Wu, F.; Yang, K.; Wang, K. Synthesis, DNA binding mode, singlet oxygen photogeneration and DNA photocleavage activity of ruthenium compounds with porphyrin-imidazo[4,5-f]phenanthroline conjugated ligand. *Appl. Organomet. Chem.* **2018**, *32* (9), No. e4468.
(89) Wang, Q.; Ng, D. K. P.; Lo, P. C. Functional aza-boron dipyrromethenes for subcellular imaging and organelle-specific photodynamic therapy. *J. Mater. Chem. B* **2018**, *6* (20), 3285−3296.
(90) Liu, P.; Wu, B. Y.; Liu, J.; Dai, Y. C.; Wang, Y. J.; Wang, K. Z. DNA binding and photocleavage properties, cellular uptake and localization, and in-vitro cytotoxicity of dinuclear ruthenium(II) complexes with varying lengths in bridging alkyl linkers. *Inorg. Chem.* **2016**, *55* (4), 1412−1422.
(91) Zhang, L.; Jiang, J. H.; Luo, J. J.; Zhang, L.; Cai, J. Y.; Teng, J. W.; Yang, P. H. A label-free electrochemiluminescence cytosensors for specific detection of early apoptosis. *Biosens. Bioelectron.* **2013**, *49*, 46−52.
(92) Cooley-Andrade, O.; Cheung, K.; Chew, A. N.; Connor, D. E.; Parsi, K. Detergent sclerosants at sub-lytic concentrations induce endothelial cell apoptosis through a caspase dependent pathway. *Apoptosis* **2016**, *21* (7), 836−845.
(93) Pang, M.; Gao, C. L.; Wu, Z. X.; Lv, N.; Wang, Z. L.; Tang, X. X.; Qu, P. Apoptosis induced by yessotoxins in Hela human cervical cancer cells in vitro. *Mol. Med. Rep.* **2010**, *3* (4), 629−634.
(94) Mukhopadhyay, S.; Singh, R. S.; Paitandi, R. P.; Sharma, G.; Koch, B.; Pandey, D. S. Influence of substituents on DNA and protein binding of cyclometalated Ir(III) complexes and anticancer activity. *Dalton Trans* **2017**, *46* (26), 8572−8585.
(95) Yin, R.; Guo, W.; Wang, H.; Du, J.; Zhou, X.; Wu, Q.; Zheng, H.; Chang, J.; Ren, N. Selective degradation of sulfonamide antibiotics by peroxymonosulfate alone: Direct oxidation and nonradical mechanisms. *Chem. Eng. J.* **2018**, *334*, 2539−2546.

DOI: 10.1021/acs.inorgchem.9b02420
Inorg. Chem. XXXX, XXX, XXX−XXX